

Online Adaptive Local Multiscale Model Reduction for Heterogeneous Problems in Perforated Domains

ERIC T. CHUNG ^{*} ^{1,2}, YALCHIN EFENDIEV ^{†2}, WING TAT LEUNG ⁴, MARIA VASILYEVA ^{2,5}, AND YATING WANG ⁴

¹*Department of Mathematics, The Chinese University of Hong Kong (CUHK), Hong Kong SAR.*

²*Department of Mathematics & Institute for Scientific Computation (ISC), Texas A&M University, College Station, TX 77843-3368, USA.*

³*Department of Mathematics, Texas A&M University, College Station, TX 77843-3368, USA.*

⁴*Department of Computational Technologies, Institute of Mathematics and Informatics, North-Eastern Federal University, Yakutsk, 677980, Republic of Sakha (Yakutia), Russia.*

May 26, 2016

Abstract

In this paper, we develop and analyze an adaptive multiscale approach for heterogeneous problems in perforated domains. We consider commonly used model problems including the Laplace equation, the elasticity equation, and the Stokes system in perforated regions. In many applications, these problems have a multiscale nature arising because of the perforations, their geometries, the sizes of the perforations, and configurations. Typical modeling approaches extract average properties in each coarse region, that encapsulate many perforations, and formulate a coarse-grid problem. In some applications, the coarse-grid problem can have a different form from the fine-scale problem, e.g., the coarse-grid system corresponding to a Stokes system in perforated domains leads to Darcy equations on a coarse grid. In this paper, we present a general offline/online procedure, which can adequately and adaptively represent the local degrees of freedom and derive appropriate coarse-grid equations. Our approaches start with the offline procedure (following [18]), which constructs multiscale basis functions in each coarse region and formulates coarse-grid equations. In [18], we presented the offline simulations without the analysis and adaptive procedures, which are needed for accurate and efficient simulations. The main contributions of this paper are (1) the rigorous analysis of the offline approach (2) the development of the online procedures and their analysis (3) the development of adaptive strategies. We present an online procedure, which allows adaptively incorporating global information and is important for a fast convergence when combined with the adaptivity. We present online adaptive enrichment algorithms for the three model problems mentioned above. Our methodology allows adding and guides constructing new online multiscale basis functions adaptively in appropriate regions. We present the convergence analysis of the online adaptive enrichment algorithm for the Stokes system. In particular, we show that the online procedure has a rapid convergence with a rate related to the number of offline basis functions, and one can obtain fast convergence by a sufficient number of offline basis functions, which are computed in the offline stage. The convergence theory can also be applied to the Laplace equation and the elasticity equation. To illustrate the performance of our method, we present numerical results with both small and large perforations. We see that only a few (1 or 2) online iterations can significantly improve the offline solution.

*Email: tschung@math.cuhk.edu.hk.

†Email: efendiev@math.tamu.edu.

1 Introduction

One important class of multiscale problems consists of problems in perforated domains (see Figure 1 for an illustration). In these problems, differential equations are formulated in perforated domains. These domains can be considered the outside of inclusions or connected bodies of various sizes. Due to the variable sizes and geometries of these perforations, solutions to these problems have multiscale features. One solution approach involves posing the problem in a domain without perforations but with a very high contrast penalty term representing the domain heterogeneities ([31, 43, 28, 32]). However, the void space can be a small portion of the whole domain and, thus, it is computationally expensive to enlarge the domain substantially.

Problems in perforated domains ([42]), as other multiscale problems, require some model reduction techniques to reduce the computational cost. The main computational cost is due to the fine grid, which needs to resolve the space between the perforations. There have been many homogenization results in perforated domains and for biphasic problems, where perforations can have distinctly different properties, e.g., [1, 36, 34, 40, 24, 41, 3, 5, 26, 38, 27, 25]. Homogenization approaches average microscale processes in perforations and outside and provide macroscale equations that differ from microscale equations. In the homogenization procedure, the local cell problems account for the microscale interaction and are solved on a fine grid. Using the solutions of the local problems, the effective properties can be computed. The resulting homogenized equations can be solved on the coarse grid with the mesh size independent of the size of the perforations for different boundary conditions and right hand sides.

To carry out the homogenization, typical assumptions on periodicity or scale separation are needed to formulate the cell problems. Some generalization to problems with random *homogeneous* pore-space geometries is introduced in a pioneering work [6], where the authors formulate assumptions, when homogenization can be done using representative volume element concepts. In these approaches, the cell problems in very large domains are formulated and the effective properties are computed using the solutions of the local problems. However, these approaches still assume that the solution space can be approximated by the solutions of directional cell problems (i.e., 2 cell problems in 2D) and the effective equations contain a limited number of effective parameters (e.g., symmetric permeability tensor). These assumptions do not hold for general heterogeneities and the effective properties may be richer (one may need more parameters). To study this, we use Generalized Multiscale Finite Element Method to identify necessary local cell solutions and obtain numerical macroscopic equations.

The main difference in developing multiscale methods for problems in perforated domains is the complexity of the domains and that many portions of the domain are excluded in the computational domain. This poses a challenging task. For typical upscaling and numerical homogenization (e.g., [42, 29]), the macroscopic equations do not contain perforations and one computes the effective properties. In multiscale methods, the macroscopic equations are numerically derived by computing multiscale basis functions [35, 7, 18]. Several multiscale methods have been developed for problems in perforated domains. Our approaches are motivated by recent works [37, 35, 9, 29, 10, 18]. In this regard, we would like to mention recent works by Le Bris and his collaborators [35], where accurate multiscale basis functions are constructed. These approaches differ from numerical homogenization and approaches that use Representative Volume Element (RVE) [20]. However, these approaches do not contain a systematic way of enriching local multiscale spaces to obtain accurate macroscale representations of the underlying fine-scale problem.

Our proposed approaches are based on the Generalized Multiscale Finite Element (GMsFEM) Framework [21, 17, 13]. The GMsFEM follows the main concept of MsFEM [23, 33, 12, 2, 4]; however, it systematically constructs multiscale basis functions for each coarse block. The main idea of the GMsFEM is to use local snapshot vectors (borrowed from global model reduction) to represent the solution space and then identify local multiscale spaces by performing appropriate local spectral problem. Using snapshot spaces is essential in problems with perforations, because the snapshots contain necessary geometry information. In the snapshot space, we perform local spectral decomposition to identify multiscale basis functions. These basis functions are derived based on the analysis presented in this paper. The local multiscale basis functions obtained as a result represent the necessary degrees of freedom to represent the microscale effects. This is in contrast to homogenization, where one apriori selects the number of cell problems.

We present the analysis of the proposed method. We focus on analyzing Stokes equations, since similar techniques can be easily extended to the elliptic and the elasticity equations. We note that in [18], we present the offline simulations for heterogeneous problems in perforated domains. In [14], the results for the mixed GMSFEM for the Laplace equation with Neumann boundary conditions are presented. The main contributions of this paper are (1) the rigorous analysis of the offline approach (2) the development of the online procedures and their analysis (3) the development of adaptive strategies. We would like to emphasize that the adaptivity and online basis construction are important for the success of multiscale methods. Indeed, in many regions, one may need only a few basis functions, while some regions may require more degrees of freedom for approximating the solution space. The online basis functions allow a fast convergence and takes into account global effects.

In the GMSFEM, the multiscale basis function construction is local and uses both local snapshot solutions and local spectral problems. In the paper, we discuss the use of randomized snapshots to reduce the offline cost associated with the snapshot space computations. One can use local oversampling techniques [22]; however, the global effects are still not used. One can accelerate the convergence by computing multiscale basis functions using a residual at the online stage [16, 11, 39]. This is done by designing new multiscale basis functions, which solve local problems using the global residual information. Online basis functions are computed adaptively and only added in regions with largest residuals. In this paper, we design online basis functions. It is important that adding online basis function decreases the error substantially and one can reduce the error in one iteration. For this reason, constructing online basis functions must guarantee that the error reduction is independent of small scales and contrast.

Constructing online basis functions follows a rigorous analysis. We show that if a sufficient number of offline multiscale basis functions are chosen, one can substantially reduce the error. This reduction is related to the eigenvalue that the corresponding eigenvector is not included in the coarse space. Thus, one can get an estimate of the error reduction apriori, which is important in practical simulations. Our analysis for the offline procedure starts with the proof of the inf-sup condition, which shows the well-posedness of our scheme. Then, we derive an a-posteriori error bound for our GMSFEM. This bound shows that the error of the solution is bounded by a computable residual and an irreducible error. This irreducible error is a measure of approximating the fine-scale space by the snapshot space. We show that the convergence rate depends on the number of offline basis functions. We note that in [18], we only present the offline simulation results without analysis. Based on the analysis, we have modified some of multiscale basis functions for Stokes' equations and moreover, introduced adaptive strategies and online basis construction techniques.

In our numerical examples, we consider two different geometries, where one case includes only a few perforations and the other case includes many perforations. We considered elliptic, elasticity, and Stokes equations and only report the results for elasticity and Stokes equations. Our results for the offline consist of adding multiscale basis functions where we observe that the error decreases as we increase the number of basis functions. However, the errors (especially those involving solution gradients) can still be large. For this reason, online basis functions are added, which can rapidly reduce the error. We summarize some of our quantitative results below.

- For elasticity equations without adaptivity, we observe that, with using 4 offline basis functions per coarse neighborhood, we can achieve 7.4 % error in L^2 norm, while the error is 26 % in H^1 norm. The results for the offline computations are similar for two different geometries.
- For Stokes equations without adaptivity, we observe that, with using 3 offline basis functions per coarse block, we can achieve 0.94 % error in L^2 norm, while the error is 8.8 % in H^1 norm. All errors are for the velocity field. The results for the offline computations are better for the case with many inclusions.
- For online simulations, we observe that the error decreases rapidly as we add one online basis functions. The error keeps decreasing fast as we increase the number of online basis functions; however, we are mostly interested in error decay when one basis function is added. We observe that the error decrease much faster if we have more than 1 initial offline basis function. For example, the error decreases only 4 times if one basis function is chosen, while the error decreases more than 10 times if 4 initial basis functions are selected (see Table 5 and 6 for the Stokes case and second geometry).

- We observe that one can effectively use adaptivity to reduce the computational cost in the online simulations. Our adaptive results show that we can achieve better accuracy for the same number of online basis functions.

The paper is organized as follows. In Section 2, we present a general setting for perforated problems, the coarse and fine grid definitions, and a general idea of the GMsFEM. In Section 3, we discuss constructing offline and online basis functions. Section 4 is devoted to numerical results. In Section 5, we present the convergence analysis for the offline and online GMsFEM. The conclusions are presented in Section 6.

2 Preliminaries

2.1 Problem setting

In this section, we present the underlying problem as stated in [18, 14] and the corresponding fine-scale and coarse-scale discretization. Let $\Omega \subset \mathbb{R}^d$ ($d = 2, 3$) be a bounded domain covered by inactive cells (for Stokes flow and Darcy flow) or active cells (for elasticity problem) \mathcal{B}^ϵ . In the paper, we will consider $d = 2$ case, though our results can be extended to $d > 2$. We use the superscript ϵ to denote quantities related to perforated domains. The active cells are where the underlying problem is solved, while inactive cells are the rest of the region. Suppose the distance between inactive cells (or active cells) is of order ϵ . Define $\Omega^\epsilon := \Omega \setminus \mathcal{B}^\epsilon$, assume it is polygonally bounded. See Figure 1 for an illustration of the perforated domain. We consider the following problem defined in a perforated domain Ω^ϵ

$$\mathcal{L}^\epsilon(w) = f, \quad \text{in } \Omega^\epsilon, \quad (1)$$

$$w = 0 \text{ or } \frac{\partial w}{\partial n} = 0, \quad \text{on } \partial\Omega^\epsilon \cap \partial\mathcal{B}^\epsilon, \quad (2)$$

$$w = g, \quad \text{on } \partial\Omega \cap \partial\Omega^\epsilon, \quad (3)$$

where \mathcal{L}^ϵ denotes a linear differential operator, n is the unit outward normal to the boundary, f and g denote given functions with sufficient regularity.

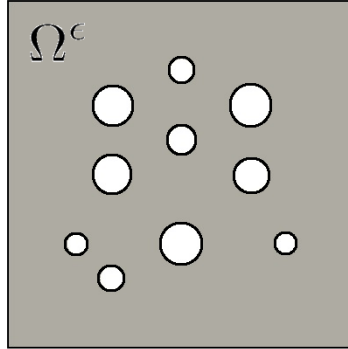


Figure 1: Illustration of a perforated domain.

Denote by $V(\Omega^\epsilon)$ the appropriate solution space, and

$$V_0(\Omega^\epsilon) = \{v \in V(\Omega^\epsilon), v = 0 \text{ on } \partial\Omega^\epsilon\}.$$

The variational formulation of Problem (1)-(3) is to find $w \in V(\Omega^\epsilon)$ such that

$$\langle \mathcal{L}^\epsilon(w), v \rangle_{\Omega^\epsilon} = (f, v)_{\Omega^\epsilon} \quad \text{for all } v \in V_0(\Omega^\epsilon),$$

where $\langle \cdot, \cdot \rangle_{\Omega^\epsilon}$ denotes a specific for the application inner product over Ω^ϵ for either scalar functions or vector functions, and $(f, v)_{\Omega^\epsilon}$ is the L^2 inner product. Some specific examples for the above abstract notations are given below.

Laplace: For the Laplace operator with homogeneous Dirichlet boundary conditions on $\partial\Omega^\epsilon$, we have

$$\mathcal{L}^\epsilon(u) = -\Delta u, \quad (4)$$

and $V(\Omega^\epsilon) = H_0^1(\Omega^\epsilon)$, $\langle \mathcal{L}^\epsilon(u), v \rangle_{\Omega^\epsilon} = (\nabla u, \nabla v)_{\Omega^\epsilon}$.

Elasticity: For the elasticity operator with a homogeneous Dirichlet boundary condition on $\partial\Omega^\epsilon$, we assume the medium is isotropic. Let $u \in (H^1(\Omega^\epsilon))^2$ be the displacement field. The strain tensor $\varepsilon(u) \in (L^2(\Omega^\epsilon))^{2 \times 2}$ is defined by

$$\varepsilon(u) = \frac{1}{2}(\nabla u + \nabla u^T).$$

Thus, the stress tensor $\sigma(u) \in (L^2(\Omega^\epsilon))^{2 \times 2}$ relates to the strain tensor $\varepsilon(u)$ such that

$$\sigma(u) = 2\mu\varepsilon + \xi \nabla \cdot u I,$$

where $\xi > 0$ and $\mu > 0$ are the Lamé coefficients. We have

$$\mathcal{L}^\epsilon(u) = -\nabla \cdot \sigma, \quad (5)$$

where $V(\Omega^\epsilon) = (H_0^1(\Omega^\epsilon))^2$ and $\langle \mathcal{L}^\epsilon(u), v \rangle_{\Omega^\epsilon} = 2\mu(\varepsilon(u), \varepsilon(v))_{\Omega^\epsilon} + \xi(\nabla \cdot u, \nabla \cdot v)_{\Omega^\epsilon}$.

Stokes: For Stokes equations, we have

$$\mathcal{L}^\epsilon(u, p) = \begin{pmatrix} \nabla p - \Delta u \\ \nabla \cdot u \end{pmatrix}, \quad (6)$$

where μ is the viscosity, p is the fluid pressure, u represents the velocity, $V(\Omega^\epsilon) = (H_0^1(\Omega^\epsilon))^2 \times L_0^2(\Omega^\epsilon)$, and

$$\langle \mathcal{L}^\epsilon(u, p), (v, q) \rangle_{\Omega^\epsilon} = \begin{pmatrix} (\nabla u, \nabla v)_{\Omega^\epsilon} & -(\nabla \cdot v, p)_{\Omega^\epsilon} \\ (\nabla \cdot u, q)_{\Omega^\epsilon} & 0 \end{pmatrix}.$$

We recall that $L_0^2(\Omega^\epsilon)$ contains functions in $L^2(\Omega^\epsilon)$ with zero average in Ω^ϵ .

In this paper, we will show the results for elasticity and Stokes equations. The results for Laplace have similar convergence analysis and computational results as those for elasticity equations, so we will omit them here.

2.2 Coarse and fine grid notations

For the numerical approximation of the above problems, we first introduce the notations of fine and coarse grids. Let \mathcal{T}^H be a coarse-grid partition of the domain Ω^ϵ with mesh size H . Here, we assume that the perforations will not split the coarse triangular element, as in this case, the coarse block will have two disconnected regions. In general, the proposed concept can be applied to this disconnected case; however, for simplicity, we avoid it and assume that every coarse-grid block is path-connected (i.e., any two points can be connected within the coarse block). Notice that, the edges of the coarse elements do not necessarily have straight edges because of the perforations (see Figure 2). By conducting a conforming refinement of the coarse mesh \mathcal{T}^H , we can obtain a fine mesh \mathcal{T}^h of Ω^ϵ with mesh size h . Typically, we assume that $0 < h \ll H < 1$, and that the fine-scale mesh \mathcal{T}^h is sufficiently fine to fully resolve the small-scale information of the domain, and \mathcal{T}^H is a coarse mesh containing many fine-scale features. Let N_v and N_e be the number of nodes and edges in coarse grid respectively. We denote by $\{x_i | 1 \leq i \leq N_v\}$ the set of coarse nodes, and $\{E_j | 1 \leq j \leq N_e\}$ the set of coarse edges.

For all the three model problems, we define a coarse neighborhood ω_i^ϵ for each coarse node x_i by

$$\omega_i^\epsilon = \cup \{K_j^\epsilon \in \mathcal{T}^H; \ x_i \in \bar{K}_j^\epsilon\}, \quad (7)$$

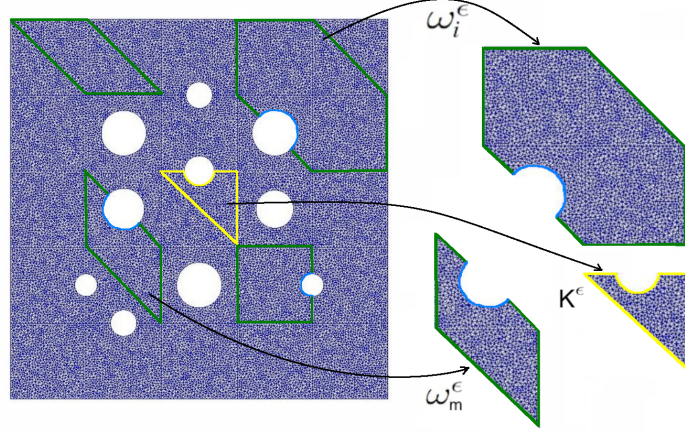


Figure 2: Illustration of coarse elements and coarse neighborhoods.

which is the union of all coarse elements having the node x_i . For the Stokes problem, additionally, we define a coarse neighborhood ω_m^ϵ for each coarse edge E_m by

$$\omega_m^\epsilon = \cup \{K_j^\epsilon \in \mathcal{T}^H; E_m \in \bar{K}_j^\epsilon\}, \quad (8)$$

which is the union of all coarse elements having the edge E_m . See Figure 2 for an illustration of the coarse neighborhoods.

On the triangulation \mathcal{T}^h , we introduce the following finite element spaces

$$V_h := \{v \in V(\Omega^\epsilon) : v|_K \in (P^k(K))^l \text{ for all } K \in \mathcal{T}^h\},$$

where, P^k denotes the polynomial of degree k ($k = 0, 1, 2$), and l ($l = 1, 2$) indicates either a scalar or a vector. Note that for the Laplace and elasticity operators, we choose $k = 1$, i.e., piecewise linear function space as our fine-scale approximation space; for Stokes problem, we use $(P^2(K))^2$ for fine-scale velocity approximation and $P^0(K)$ for fine-scale pressure approximation. We use Q_h to denote the space for pressure.

We will then obtain the fine-scale solution $u \in V_h$ by solving the following variational problem

$$\langle \mathcal{L}^\epsilon(u), v \rangle_{\Omega^\epsilon} = (f, v)_{\Omega^\epsilon}, \quad \text{for all } v \in V_h \quad (9)$$

for Laplace and elasticity, and obtain the fine-scale solution $(u, p) \in V_h \times Q_h$ by solving the following variational problem

$$\langle \mathcal{L}^\epsilon(u, p), (v, q) \rangle_{\Omega^\epsilon} = ((f, 0), (v, q))_{\Omega^\epsilon}, \quad \text{for all } (v, q) \in V_h \times Q_h \quad (10)$$

for the Stokes system. These solutions are used as reference solutions to test the performance of our schemes.

2.3 General idea of GMsFEM

Now, we present the general idea of GMsFEM [21, 30, 16]. We divide the computations into offline and online stages.

Offline stage. The construction of offline space usually contains two steps:

- Construction of a snapshot space that will be used to compute an offline space.
- Construction of a small dimensional offline space by performing a dimension reduction in the snapshot space.

From the above process, we will get a set of basis functions $\{\Psi_i^{\text{off}}\}$ such that each Ψ_i^{off} is supported in some coarse neighborhood w_i^ϵ . Also, the basis functions satisfy a partition of unity property.

Once the bases are constructed, we define the coarse function space as

$$V_{\text{off}} := \text{span}\{\Psi_i^{\text{off}}\}_{i=1}^M,$$

where M is the number of coarse basis functions.

In the offline stage of GmsFEM, we seek an approximation $u_{\text{ms}} = \sum_{i=1}^M c_i \Psi_i^{\text{off}}$ in V_{off} , which satisfies the coarse-scale offline formulation,

$$\langle \mathcal{L}^\epsilon(u_{\text{ms}}), v \rangle_{\Omega^\epsilon} = (f, v)_{\Omega^\epsilon}, \quad \text{for all } v \in V_{\text{off}}. \quad (11)$$

Here, the bilinear forms $\langle \mathcal{L}^\epsilon(u_{\text{ms}}), v \rangle_{\Omega^\epsilon}$ are as defined before, and $(f, v)_{\Omega^\epsilon}$ is the L^2 inner product.

Online stage. Now, we will turn our attention to the online computation. At the enrichment level m , denote by V_{ms}^m and u_{ms}^m the corresponding GmsFEM space and solution, respectively. The online basis functions are constructed based on the residuals of the current multiscale solution u_{ms}^m . To be specific, one can compute the local residual $R_i = (f, v)_{\omega_i^\epsilon} - \langle \mathcal{L}^\epsilon(u_{\text{ms}}^m), v \rangle_{\omega_i^\epsilon}$ in each coarse neighborhood ω_i^ϵ . For the coarse neighborhoods where the residuals are large, we can add one or more basis functions by solving

$$\mathcal{L}^\epsilon(\phi_i^{\text{on}}) = R_i.$$

Adding the online basis in the solution space, we will get a new coarse function space V_{ms}^{m+1} . The new solution u_{ms}^{m+1} will be found in this approximation space. This iterative process is stopped when some error tolerance is achieved. The accuracy of the GmsFEM relies on the coarse basis functions. We shall present the construction of suitable basis functions in both offline and online stages for the differential operators defined above.

3 The construction of offline and online basis functions

In this section, we describe the construction of offline and online basis for elasticity problem and Stokes problem.

In the offline computation, we first construct a snapshot space V_{snap}^i for each coarse neighborhood ω_i^ϵ . Construction of the snapshot space involves solving the local problems for various choices of input parameters. The offline space V_{off} is then constructed via a dimension reduction in the snapshot space using an auxiliary spectral decomposition. The main objective is to seek a subspace of the snapshot space such that it can approximate any element of the snapshot space in an appropriate sense defined via auxiliary bilinear forms. Based on the residual of the current solution, we enrich the solution space by adding some online functions to enhance the accuracy of the solution. The precise construction of offline and online basis will be presented for different applications.

3.1 Elasticity Problem

In this section, we will consider the elasticity problem (5) with a homogeneous Dirichlet boundary condition.

3.1.1 Snapshot Space

The snapshot space for elasticity problem consists of extensions of the fine-grid functions δ_k^h in ω_i^ϵ . Here $\delta_k^h = 1$ at the fine node $x_k \in \partial\omega_i^\epsilon \setminus \partial\mathcal{B}^\epsilon$, $\delta_k^h = 0$ at other fine nodes $x_j \in \partial\omega_i^\epsilon \setminus \partial\mathcal{B}^\epsilon$, and $\delta_k^h = 0$ in $\partial\mathcal{B}^\epsilon$. Let V_h^i be the restriction of the fine grid space V_h in ω_i^ϵ and $V_{h,0}^i \subset V_h^i$ be the set of functions that vanish on $\partial\omega_i^\epsilon$. We will find $u_k^i \in V_h^i$ with $\text{supp}(u_k^i) \subset \omega_i^\epsilon$ by solving the following problems on a fine grid

$$\int_{\omega_i^\epsilon} \left(2\mu \varepsilon(u_k^i) : \varepsilon(v) + \xi \nabla \cdot u_k^i \nabla \cdot v \right) dx = 0, \quad \forall v \in V_{h,0}^i, \quad (12)$$

with boundary conditions

$$u_k^i = 0 \quad \text{on} \quad \partial\omega_i^\epsilon \cap \partial\mathcal{B}^\epsilon, \quad u_k^i = (\delta_j^i, 0) \quad \text{or} \quad (0, \delta_j^i) \quad \text{on} \quad \partial\omega_i^\epsilon.$$

We will collect the solutions of the above local problems to generate the snapshot space. Let $\psi_k^{i,\text{snap}} := u_k^i$ and define the snapshot space by

$$V_{\text{snap}} = \text{span}\{\psi_k^{i,\text{snap}} : 1 \leq k \leq J_i, 1 \leq i \leq N_v\},$$

where J_i is the number of snapshot basis in ω_i^ϵ , and N_v is the number of nodes. To simplify notations, let $M_{\text{snap}} = \sum_{i=1}^N J_i$ and write

$$V_{\text{snap}} = \text{span}\{\psi_i^{\text{snap}} : 1 \leq i \leq M_{\text{snap}}\}.$$

3.1.2 Offline space

This section is devoted to the construction of the offline space via a spectral decomposition. We will consider the following eigenvalue problems in the space of snapshots:

$$A^{i,\text{off}} \Psi_k^{i,\text{off}} = \lambda_k^{i,\text{off}} S^{i,\text{off}} \Psi_k^{i,\text{off}}, \quad (13)$$

where

$$\begin{aligned} A^{i,\text{off}} &= a_i(\psi_m^{i,\text{snap}}, \psi_n^{i,\text{snap}}) = \int_{\omega_i^\epsilon} \left(2\mu \epsilon(\psi_m^{i,\text{snap}}) : \epsilon(\psi_n^{i,\text{snap}}) + \xi \nabla \cdot \psi_m^{i,\text{snap}} \nabla \cdot \psi_n^{i,\text{snap}} \right), \\ S^{i,\text{off}} &= s_i(\psi_m^{i,\text{snap}}, \psi_n^{i,\text{snap}}) = \int_{\omega_i^\epsilon} (\xi + 2\mu) \psi_m^{i,\text{snap}} \cdot \psi_n^{i,\text{snap}}. \end{aligned} \quad (14)$$

We assume that the eigenvalues are arranged in the increasing order. To simplify notations, we write $\lambda_k^i = \lambda_k^{i,\text{off}}$.

To generate the offline space, we choose the smallest M_i eigenvalues from Equation (13) and form the corresponding eigenfunctions in the respective snapshot spaces by setting $\Phi_k^{i,\text{off}} = \sum_j \Psi_{kj}^{i,\text{off}} \psi_j^{i,\text{snap}}$, for $k = 1, \dots, M_i$, where $\Psi_{kj}^{i,\text{off}}$ are the coordinates of the vector $\Psi_k^{i,\text{off}}$. The offline space is defined as the span of $\chi_i \Phi_k^{i,\text{off}}$, namely,

$$V_{\text{off}} = \text{span}\{\chi_i \Phi_l^{i,\text{off}} : 1 \leq l \leq l_i, 1 \leq i \leq N_v\},$$

where l_i is the number of snapshot basis in ω_i^ϵ , and $\{\chi_i\}$ is a set of partition of unity functions for the coarse grid. One can take $\{\chi_i\}$ as the standard hat functions or standard multiscale basis functions. To simplify notations further, let $M = \sum_{i=1}^N l_i$ and write

$$V_{\text{off}} = \text{span}\{\chi_i \Phi_i^{\text{off}} : 1 \leq i \leq M\}.$$

3.1.3 Online adaptive method

By the offline computation, we construct multiscale basis functions that can be used for any input parameters to solve the problem on the coarse grid. In the earlier works [15, 16], the online method for the diffusion equation with heterogeneous coefficients has been proposed. In this section, we consider the construction of the online basis functions for elasticity problem in perforated domains and present an adaptive enrichment algorithm. We use the index $m \geq 1$ to represent the enrichment level. The online basis functions are computed based on some local residuals for the current multiscale solution $u_{\text{ms}}^m \in V_{\text{ms}}^m$, where we use V_{ms}^m to denote the corresponding space that can contain both offline and online basis functions.

Let $V_{\text{ms}}^{m+1} = V_{\text{ms}}^m + \text{span}\{\phi^{\text{on}}\}$ be the new approximate space that constructed by adding online basis $\phi^{\text{on}} \in V_{h,0}^i$ on the i -th coarse neighborhood ω_i^ϵ . For each coarse grid neighborhood ω_i^ϵ , we define the residual R_i as a linear functional on $V_{h,0}^i$ such that

$$R_i(v) = \int_{\omega_i^\epsilon} f v dx - \int_{\omega_i^\epsilon} \left(2\mu \varepsilon(u_{\text{ms}}^m) : \varepsilon(v) + \xi \nabla \cdot u_{\text{ms}}^m \nabla \cdot v \right) dx, \quad \forall v \in V_{h,0}^i.$$

The norm of R_i is defined as

$$\|R_i\|_{(V_h^i)^*} = \sup_{v \in V_{h,0}^i} \frac{|R_i(v)|}{a_i(v, v)^{\frac{1}{2}}},$$

where $a_i(v, v) = \int_{\omega_i^\epsilon} \left(2\mu \varepsilon(v) : \varepsilon(v) + \xi \nabla \cdot v \nabla \cdot v \right) dx$.

For the computation of this norm, according to the Riesz representation theorem, we can first compute ϕ^{on} as the solution of following problem

$$\int_{\omega_i^\epsilon} \left(2\mu \varepsilon(\phi^{\text{on}}) : \varepsilon(v) + \xi \nabla \cdot \phi^{\text{on}} \nabla \cdot v \right) dx = \int_{\omega_i^\epsilon} f v dx - \int_{\omega_i^\epsilon} \left(2\mu \varepsilon(u_{\text{ms}}^m) : \varepsilon(v) + \xi \nabla \cdot u_{\text{ms}}^m \nabla \cdot v \right) dx, \quad \forall v \in V_{h,0}^i \quad (15)$$

and take $\|R_i\|_{(V_h^i)^*} = a_i(\phi^{\text{on}}, \phi^{\text{on}})^{\frac{1}{2}}$.

For the construction of the adaptive online basis functions, we use the following error indicators to access the quality of the solution. In those non-overlapping coarse grid neighborhoods ω_i^ϵ with large residuals, we enrich the space by finding online basis $\phi^{\text{on}} \in V_{h,0}^i$ using equation (15).

- *Indicator 1.* The error indicator based on local residual

$$\eta_i = \|R_i\|_{(V_h^i)^*}^2 \quad (16)$$

- *Indicator 2.* The error indicator based on local residual and eigenvalue

$$\eta_i = (\lambda_{l_i+1}^{\omega_i})^{-1} \|R_i\|_{(V_h^i)^*}^2 \quad (17)$$

Now we present the adaptive online algorithm. We start with enrichment iteration number $m = 0$ and choose $\theta \in (0, 1)$. Suppose the initial number of offline basis functions is $l_i^m (m = 1)$ for each coarse grid neighborhood ω_i^ϵ , and the multiscale space is $V_{\text{ms}}^m (m = 1)$. For $m = 1, 2, \dots$

- *Step 1.* Find u_{ms}^m in V_{ms}^m such that

$$\int_{\omega_i^\epsilon} \left(2\mu \varepsilon(u_{\text{ms}}^m) : \varepsilon(v) + \xi \nabla \cdot u_{\text{ms}}^m \nabla \cdot v \right) dx = \int_{\omega_i^\epsilon} f v, \quad \forall v \in V_{\text{ms}}^m.$$

- *Step 2.* Compute error indicators (η_i) for every coarse grid neighborhoods ω_i^ϵ and sort them in decreasing order $\eta_1 \geq \eta_2 \geq \dots \geq \eta_N$.
- *Step 3.* Select coarse grid neighborhoods ω_i^ϵ , where enrichment is needed. We take smallest k such that

$$\theta \sum_{i=1}^{N_v} \eta_i \leq \sum_{i=1}^k \eta_i.$$

- *Step 4.* Enrich the space by adding online basis functions. For each ω_i^ϵ , where $i = 1, 2, \dots, k$, we find $\phi^{\text{on}} \in V_{h,0}^i$ by solving (15). The resulting space is denoted by V_{ms}^{m+1} .

We repeat the above procedure until the global error indicator is small or we have certain number of basis functions.

3.2 Stokes problem

In the above section, we presented the online procedure for the elasticity equations. In this section, we present the constructions of snapshot, offline and online basis functions for the Stokes problem.

3.2.1 Snapshot space

Snapshot space is a space which contains an extensive set of basis functions that are solutions of local problems with all possible boundary conditions up to fine-grid resolution. To get snapshot functions, we solve the following problem on the coarse neighborhood ω_i^ϵ : find (u_l^i, p_l^i) (on a fine grid) such that

$$\begin{aligned} \int_{\omega_i^\epsilon} \nabla u_l^i : \nabla v dx - \int_{\omega_i^\epsilon} p_l^i \operatorname{div}(v) dx &= 0, \quad \forall v \in V_{h,0}^i, \\ \int_{\omega_i^\epsilon} q \operatorname{div}(u_l^i) dx &= \int_{\omega_i^\epsilon} c q dx, \quad \forall q \in Q_h^i, \end{aligned} \quad (18)$$

with boundary conditions

$$u_l^i = (0, 0), \text{ on } \partial\mathcal{B}^\epsilon, \quad u_l^i = (\delta_l^i, 0) \text{ or } (0, \delta_l^i), \text{ on } \partial\omega_i^\epsilon \setminus \partial\mathcal{B}^\epsilon,$$

where function δ_l^i is a piecewise constant function such that it has value 1 on e_l and value 0 on other fine-grid edges. Notice that $\omega_i^\epsilon \setminus \partial\mathcal{B}^\epsilon = \cup_{l=1}^{S_i} e_l$, where e_l are the fine-grid edges and S_i is the number of these fine grid edges on $\omega_i^\epsilon \setminus \partial\mathcal{B}^\epsilon$. In (18), we define V_h^i and Q_h^i as the restrictions of the fine grid space in ω_i^ϵ and $V_{h,0}^i \subset V_h^i$ be functions that vanish on $\partial\omega_i^\epsilon$. Notice that u_l^i and p_l^i are supported in ω_i^ϵ . We remark that the constant c in (18) is chosen by compatibility condition, $c = \frac{1}{|\omega_i^\epsilon|} \int_{\partial\omega_i^\epsilon \setminus \partial\mathcal{B}^\epsilon} u_l^i \cdot n_i ds$. We emphasize that, for the Stokes problem, we will solve (18) in both node-based coarse neighborhoods (7) and edge-based coarse neighborhoods (8).

The collection of the solutions of above local problems generates the snapshot space, $\psi_l^{i,\text{snap}} = u_l^i$ in ω_i^ϵ :

$$V_{\text{snap}} = \{\psi_l^{i,\text{snap}} : 1 \leq l \leq 2S_i, 1 \leq i \leq (N_e + N_v)\},$$

where we recall that N_e is the number of coarse-grid edges and N_v is the number of coarse-grid nodes.

3.2.2 Offline Space

We perform a space reduction in the snapshot space through the use of a local spectral problem in ω_i^ϵ . The purpose of this is to determine the dominant modes in the snapshot space and to obtain a small dimension space for the approximation the solution.

We consider the following local eigenvalue problem in the snapshot space

$$A^{i,\text{off}} \Psi_k = \lambda_k^{i,\text{off}} S^{i,\text{off}} \Psi_k^{i,\text{off}}, \quad (19)$$

where

$$\begin{aligned} A^{i,\text{off}} &= a_i(\psi_m^{i,\text{snap}}, \psi_n^{i,\text{snap}}) \\ S^{i,\text{off}} &= s_i(\psi_m^{i,\text{snap}}, \psi_n^{i,\text{snap}}) \end{aligned}$$

and

$$a_i(u, v) = \int_{\omega_i^\epsilon} \nabla u : \nabla v dx, \quad \text{and} \quad s_i(u, v) = \int_{\omega_i^\epsilon} |\nabla \chi_i|^2 u \cdot v dx$$

and χ_i will be specified later. Note that the above spectral problem is solved in the local snapshot space corresponding to the neighborhood domain ω_i^ϵ . We arrange the eigenvalues in the increasing order, and choose the first M_i eigenvalues and take the corresponding eigenvectors $\Psi_k^{i,\text{off}}$, for $k = 1, 2, \dots, M_i$, to form

the basis functions, i.e., $\tilde{\Phi}_k^{i,\text{off}} = \sum_j \Psi_{kj}^{i,\text{off}} \psi_j^{i,\text{snap}}$, where $\Psi_{kj}^{i,\text{off}}$ are the coordinates of the vector $\Psi_k^{i,\text{off}}$. We define

$$\tilde{V}_{\text{off}}^i = \text{span}\{\tilde{\Phi}_k^{i,\text{off}}, \quad k = 1, 2, \dots, 2S_i\}. \quad (20)$$

For construction of conforming offline space, we need to multiply the functions $\tilde{\Phi}_k^{i,\text{off}} = (\tilde{\Phi}_{x_1,k}^{i,\text{off}}, \tilde{\Phi}_{x_2,k}^{i,\text{off}})$ by a partition of unity function χ_i . We remark that the partition of unity functions $\{\chi_i\}$ are defined with respect to the coarse nodes and the mid-points of coarse edges. One can choose $\{\chi_i\}$ as the standard multiscale finite element basis. However, upon multiplying by partition of unity functions, the resulting basis functions do not have constant divergence any more, which affects the stability of the scheme. To resolve this problem, we solve two local optimization problems in every coarse element $K_j^i \subset \omega_i^\epsilon$:

$$\min \left\| \nabla \Phi_{x_1,k}^{i,\text{off}} \right\|_{L^2(K_j^i)} \quad \text{such that} \quad \text{div}(\Phi_{x_1,k}^{i,\text{off}}) = \frac{1}{|K_j^i|} \int_{\partial K_j^i} (\chi_i \tilde{\Phi}_{x_1,k}^{i,\text{off}}, 0) \cdot n_i \, ds, \quad \text{in } K_j^i \quad (21)$$

with $\Phi_{x_1,k}^{i,\text{off}} = (\chi_i \tilde{\Phi}_{x_1,k}^{i,\text{off}}, 0)$, on ∂K_j^i , and

$$\min \left\| \nabla \Phi_{x_2,k}^{i,\text{off}} \right\|_{L^2(K_j^i)} \quad \text{such that} \quad \text{div}(\Phi_{x_2,k}^{i,\text{off}}) = \frac{1}{|K_j^i|} \int_{\partial K_j^i} (0, \chi_i \tilde{\Phi}_{x_2,k}^{i,\text{off}}) \cdot n_i \, ds \quad \text{in } K_j^i, \quad (22)$$

with $\Phi_{x_2,k}^{i,\text{off}} = (0, \chi_i \tilde{\Phi}_{x_2,k}^{i,\text{off}})$, on ∂K_j^i . We write that $\Phi_{x_1,k}^{i,\text{off}} = \mathcal{H}(\chi_i \tilde{\Phi}_{x_1,k}^{i,\text{off}})$ and $\Phi_{x_2,k}^{i,\text{off}} = \mathcal{H}(\chi_i \tilde{\Phi}_{x_2,k}^{i,\text{off}})$, where $\mathcal{H}(v)$ is the *Stokes extension* of the function v .

Combining them, we obtain the global offline space:

$$V_{\text{off}} = \text{span}\{\Phi_{x_1,k}^{i,\text{off}} \text{ and } \Phi_{x_2,k}^{i,\text{off}} : \quad 1 \leq i \leq (N_e + N_v) \text{ and } 1 \leq k \leq M_i\}.$$

Using a single index notation, we can write

$$V_{\text{off}} = \text{span}\{\Phi_i^{\text{off}}\}_{i=1}^{N_u},$$

where $N_u = \sum_{i=1}^{N_e+N_v} M_i$. This space will be used as the approximation space for the velocity. For coarse approximation of pressure, we will take Q_{off} to be the space of piecewise constant functions on the coarse mesh.

3.2.3 Online Adaptive Method

Similar to Section 3.1.3, we will define the online velocity basis for Stokes problem. For each coarse grid neighborhood ω_i^ϵ , we define the residual R_i as a linear functional on V^i such that

$$R_i(v) = \int_{\omega_i^\epsilon} f \cdot v \, dx - \int_{\omega_i^\epsilon} \nabla u_{\text{ms}}^m : \nabla v \, dx + \int_{\omega_i^\epsilon} p_{\text{ms}}^m \text{div}(v) \, dx, \quad \forall v \in V^i \quad (23)$$

where $(u_{\text{ms}}^m, p_{\text{ms}}^m)$ is the multiscale solution at the enrichment level m , and $V^i = (H_0^1(\omega_i^\epsilon))^2$. The norm of R_i is defined as

$$\|R_i\|_{(V^i)^*} = \sup_{v \in V^i} \frac{|R_i(v)|}{\|v\|_{H^1(\omega_i^\epsilon)}}. \quad (24)$$

We will then use indicators (16) and (17) for our adaptive enrichment method. For the computation of online basis $\phi_i^{\text{on}} \in V_{h,0}^i$, we solve the following problem

$$\begin{aligned} \int_{\omega_i^\epsilon} \nabla \phi_i^{\text{on}} : \nabla v \, dx - \int_{\omega_i^\epsilon} p^{\text{on}} \text{div}(v) \, dx &= R_i(v), \quad \forall v \in V_{h,0}^i, \\ \int_{\omega_i^\epsilon} \text{div}(\phi_i^{\text{on}}) q \, dx &= 0, \quad \forall q \in Q_{\text{off}}. \end{aligned} \quad (25)$$

The adaptivity procedure follows the one presented in Section 3.1.3.

3.3 Randomized snapshots

In the above construction, the local problems are solved for every boundary node. This procedure is expensive and may not be practical. However, one can use the idea of randomized snapshots (as in [8]) and reduce the cost substantially. In randomized snapshots, one computes a few more snapshots compared to the required number of multiscale basis functions. E.g., we compute $n + 4$ snapshots for n multiscale basis functions.

To be more specific, we first generate inexpensive snapshots using random boundary conditions. Instead of solving the local problem (12) and (18) for each fine boundary degree of freedom, we solve a small number of local problems with boundary conditions:

$$\begin{aligned} u_k^{+,i} &= (r_l^i, 0) \quad \text{or} \quad (0, r_l^i) \quad \text{on} \quad \partial\omega_i^{+, \epsilon} \setminus \partial\mathcal{B}^\epsilon, \\ u_k^{+,i} &= (0, 0) \quad \text{on} \quad \partial\mathcal{B}^\epsilon. \end{aligned}$$

Here r_l^i are independent identically distributed (i.i.d.) standard Gaussian random vectors defined on the fine degree freedom of the boundary. Notice that we will solve for $u_k^{+,i}$ in a larger domain, the oversampling domain $\omega_i^{+, \epsilon}$. The oversampling technique is used to avoid the effects of randomized boundaries. After removing dependence, we finally get our snapshot basis by taking the restriction of $u_k^{+,i}$ in ω_i^ϵ , i.e., $u_k^i = u_k^{+,i}|_{\omega_i^\epsilon}$.

In Section 4, we will take the Stokes problem as an example and show the numerical results for randomized snapshots.

4 Numerical results

In this section, we show simulation results using the framework of online adaptive GMsFEM presented in Section 2.3 for elasticity equations and Stokes equations. We set $\Omega = [0, 1] \times [0, 1]$ and use two types of perforated domains as illustrated in Figure 3, where the perforated regions \mathcal{B}^ϵ are circular. We have also used perforated regions of other shapes instead and obtained similar results. The computational domain is discretized coarsely using uniform triangulation, where the coarse mesh size $H = \frac{1}{10}$ for elasticity problem and $H = \frac{1}{5}$ for Stokes problem. Furthermore, nonuniform triangulation is used inside each coarse triangular element to obtain a finer discretization. Examples of this triangulation are displayed also in Figure 3.

First we will choose a fixed number of offline basis (initial basis) for every coarse neighborhood, and obtain corresponding offline space V_{off} , which is also denoted by V_{ms}^1 . Then, we perform the online iterations on non-overlapping coarse neighborhoods to obtain enriched space V_{ms}^m , $m \geq 1$. We will add online basis both with adaptivity and without adaptivity and compare the results. All the errors are in percentage. We note that our approaches are designed to explore the sparsity and the adaptivity in the solution space and our main emphasis is on the construction of coarse spaces. Our numerical results will show the approximation of the fine-scale solution for different dimensional coarse spaces.

4.1 Elasticity equations in perforated domain

We consider the elasticity operator (5). We use zero displacements $u = 0$ on the inclusions, $u_1 = 0, \sigma_2 = 0$ on the left boundary, $\sigma_1 = 0, u_2 = 0$ on the bottom boundary and $\sigma_1 = 0, \sigma_2 = 0$ on the right and top boundaries. Here, $u = (u_1, u_2)$ and $\sigma = (\sigma_1, \sigma_2)$. The source term is defined by $f = (10^7, 10^7)$, the elastic modulus is given by $E = 10^9$, Poisson's ratio is $\nu = 0.22$, where

$$\mu = \frac{E}{2(1 + \nu)}, \quad \xi = \frac{E\nu}{(1 + \nu)(1 - 2\nu)}.$$

We use the following error quantities to measure the performance of the online adaptive GMsFEM

$$\|e\|_{L^2} = \|e_u\|_{L^2(\Omega^\epsilon)} = \frac{\|(\xi + 2\mu)(u - u_{\text{ms}})\|_{L^2(\Omega^\epsilon)}}{\|(\xi + 2\mu)u\|_{L^2(\Omega^\epsilon)}}, \quad \|e\|_{H^1} = \|e_u\|_{H^1(\Omega^\epsilon)} = \sqrt{\frac{\langle \mathcal{L}^\epsilon(u - u_{\text{ms}}), u - u_{\text{ms}} \rangle_{\Omega^\epsilon}}{\langle \mathcal{L}^\epsilon(u), u \rangle_{\Omega^\epsilon}}},$$

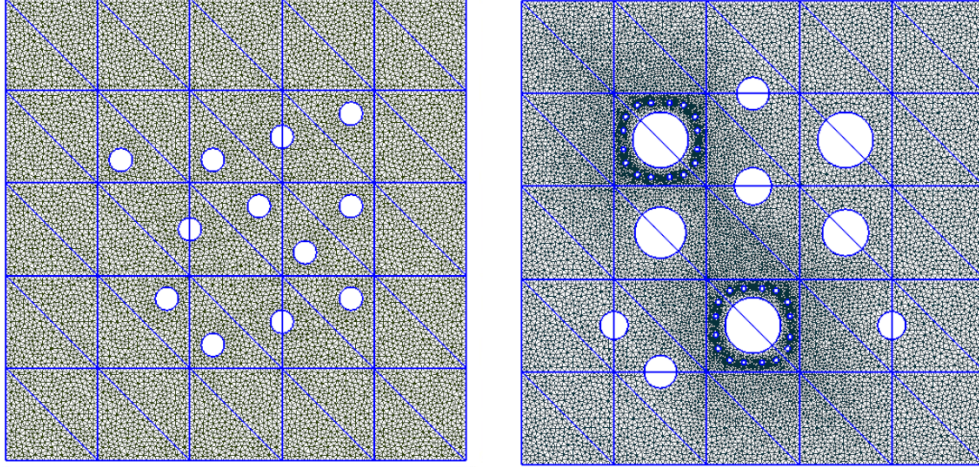


Figure 3: Two heterogeneous perforated medium used in the simulations.

where u and u_{ms} are the fine and coarse solutions, respectively, and $\langle \mathcal{L}^\epsilon(u), v \rangle_{\Omega^\epsilon} = 2\mu \langle \epsilon(u), \epsilon(v) \rangle_{\Omega^\epsilon} + \xi \langle \nabla \cdot u, \nabla \cdot v \rangle_{\Omega^\epsilon}$. Note that the reference solution u needs a full fine scale computation. The fine grid DOF is 13262 for the domain with small perforations (left in Figure 3) and 21986 for the domain with big perforations (right in Figure 3).

The fine-scale solution and coarse-scale solution corresponding to the two different perforated domains in Figure 3 are presented in Figures 4 and 5. Fine solutions are shown on the left of the figure, coarse offline solutions are in the middle and online solutions are on the right. In Tables 1 and 2, we present the convergence history when the problem is solved in two different perforated domain with one, two and four initial bases in the left, middle and right column, respectively. Each column shows the error behavior when the online method is applied without adaptivity, with adaptivity using Indicator 1 (see (16)) and with adaptivity using Indicator 2 (see (17)).

Numerical results for the first perforated domain are displayed in Figure 4. We observe that the offline solution is close to the fine-scale solution; however, there are some missing features in the offline solution. For example, the low values of the solution for a connected regions around circular inclusions, while this is not the case for the fine-scale solution. Also, we observe that the offline solution does not capture the low values of the solution near the inclusions. On the other hand, the solution using the online procedure with approximately the same number of degrees of freedom as the offline solution has very good accuracy. From Table 1, we observe that when using one initial basis, the L^2 and energy error reduce to 1.3% and 5.82% respectively after one online iteration in the case without adaptivity. However, if we select two initial bases, the L^2 and energy error can be reduced to 0.567% and 2.92% respectively after one online iteration, which is almost half of the errors for one initial basis situation. When the number of basis is fixed, it shows that adding online basis can reduce the error more effectively than adding offline basis. For example, when we use two offline basis and two online basis, the energy error is 0.369%; while when we select four offline basis, the energy error is 26.703%. Comparison of the error behavior between solving with and without adaptivity in this table shows that, error is smaller under the similar DOF when adaptive online method is applied. For example, if we start with one initial basis, the energy error is 5.482% with DOF 500 when online method is applied without adaptivity, but the energy error becomes 2.589% with DOF 536 when online adaptive method is applied. When we solve with the adaptivity, we observe that the first indicator (see (16)) is more effective when one initial basis is selected. However, if we start with two or four initial bases, the second indicator (see (17)) gives us slightly better results. The smallest eigenvalues are $\Lambda_{min} = 31.4, 79.9, 204.8$ when one, two and four initial basis are used.

In Figure 5, we test with a different perforated domain where the circular inclusions are larger compared

to the domain in Figure 4 and extremely small inclusions are set around some big ones. Comparing the offline and fine solution, we notice that some features of solution in the interior of the domain are missing, and the errors around the boundary are large. However, the online solution fix these problems well and show much better accuracy. Looking at Table 2, we observe that as we select more initial basis, the error decreases faster after one online iteration. For example, when one online iteration is applied without adaptivity, the H^1 error reduces 8.5 times if we use one initial basis, yet it reduces around 12 times if we use two initial basis. Considering the convergence behavior of online method with adaptivity against the online method without adaptivity, we see that the adaptivity is important. For instance, in a similar DOF of 1300 in the case of four initial basis used, the H^1 error 10^{-5} without adaptivity, while it is only 10^{-6} with adaptivity.

DOF (# iter)	$\ e\ _{L^2}$	$\ e\ _{H^1}$
without adaptivity		
338	29.269	53.691
500 (1)	1.300	5.482
662 (2)	0.082	0.450
824 (3)	0.010	0.069
986 (4)	0.0009	0.007
with adaptivity, $\eta_i^2 = r_i^2$		
338	29.269	53.691
510 (3)	0.567	3.115
654 (6)	0.042	0.306
852 (10)	0.001	0.013
1014 (13)	0.0001	0.0008
with adaptivity, $\eta_i^2 = r_i^2 \lambda_{i+1}^{-1}$		
338	29.269	53.691
536 (4)	0.474	2.589
684 (7)	0.039	0.285
846 (10)	0.003	0.023
1002 (13)	0.0002	0.001

DOF (# iter)	$\ e\ _{L^2}$	$\ e\ _{H^1}$
without adaptivity		
412	10.652	32.862
574 (1)	0.567	2.921
736 (2)	0.049	0.369
898 (3)	0.005	0.047
1060 (4)	0.0005	0.004
with adaptivity, $\eta_i^2 = r_i^2$		
412	10.652	32.862
584 (3)	0.416	2.285
740 (6)	0.029	0.236
932 (10)	0.001	0.009
1190 (15)	1.685e-05	0.0001
with adaptivity, $\eta_i^2 = r_i^2 \lambda_{i+1}^{-1}$		
412	10.652	32.862
570 (3)	0.437	2.519
730 (6)	0.031	0.252
924 (10)	0.001	0.009
1072 (13)	8.772e-05	0.0006

DOF (# iter)	$\ e\ _{L^2}$	$\ e\ _{H^1}$
without adaptivity		
648	7.414	26.703
810 (1)	0.479	2.509
972 (2)	0.046	0.368
1134 (3)	0.004	0.043
1296 (4)	0.0005	0.004
with adaptivity, $\eta_i^2 = r_i^2$		
648	7.414	26.703
808 (3)	0.303	1.977
980 (6)	0.022	0.192
1144 (9)	0.001	0.016
1302 (12)	0.0001	0.001
with adaptivity, $\eta_i^2 = r_i^2 \lambda_{i+1}^{-1}$		
648	7.414	26.703
808 (3)	0.300	1.776
976 (6)	0.019	0.173
1174 (10)	0.0006	0.005
1338 (13)	3.492e-05	0.0002

Table 1: Elasticity problem in the perforated domain with small inclusions (Figure 3, left). One (Left), Two (Middle) and Four (Right) offline basis functions ($\theta = 0.7$).

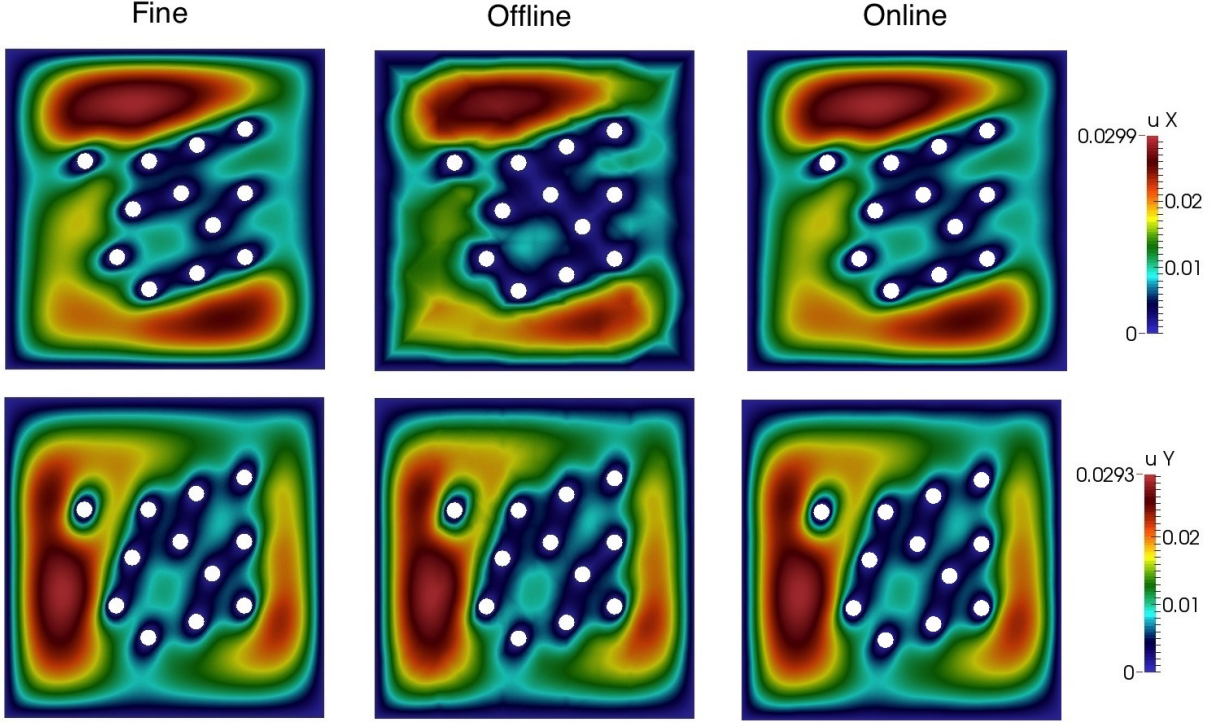


Figure 4: Elasticity problem in the perforated domain with small inclusions (Figure 3, left). Comparison of solutions in: Fine scale (left) $DOF = 13262$, Coarse-scale offline, $DOF = 412$ (middle), Coarse-scale online without adaptivity, $DOF = 574$ (right). Top: u_1 . Bottom: u_2 .

4.2 Stokes equations in perforated domain

In our final example, we consider the Stokes operator (6) with zero velocity $u = (0, 0)$ on $\partial\Omega^\epsilon \cap \partial\mathcal{B}^\epsilon$ and $\frac{\partial u}{\partial n} = (0, 0)$ on $\partial\Omega$, and source term $f = (1, 1) \in \Omega^\epsilon$. For the fine-scale approximation of the Stokes problem, we use P_2 elements for velocity and piecewise constants for pressure. To improve the accuracy of multiscale solutions, we have enriched velocity spaces by adding online velocity basis.

The errors will be measured in relative L^2 and H^1 norms for velocity and L^2 norm for pressure

$$\begin{aligned} \|e_u\|_{L^2} &= \|e_u\|_{L^2(\Omega^\epsilon)} = \frac{\|u - u_{ms}\|_{L^2(\Omega^\epsilon)}}{\|u\|_{L^2(\Omega^\epsilon)}}, \quad \|e_u\|_{H^1} = \|e_u\|_{H^1(\Omega^\epsilon)} = \frac{\|u - u_{ms}\|_{H^1(\Omega^\epsilon)}}{\|u\|_{H^1(\Omega^\epsilon)}}, \\ \|e_p\|_{L^2} &= \frac{\|\bar{p} - p_{ms}\|_{L^2(\Omega^\epsilon)}}{\|\bar{p}\|_{L^2(\Omega^\epsilon)}}, \end{aligned}$$

where (u, p) and (u_{ms}, p_{ms}) are fine-scale and coarse-scale solutions, respectively for velocity and pressure, and \bar{p} is the cell average of the fine scale pressure, that is, $\bar{p} = \frac{1}{|K_i^\epsilon|} \int_{K_i^\epsilon} p$ for all $K_i^\epsilon \in \mathcal{T}^H$. Notice that we solve the reference solution (u, p) on a full fine grid. The fine grid DOF is 77524 for the domain with small perforations (left in Figure 3) and 101386 for the domain with big perforations (right in Figure 3).

4.2.1 Randomized snapshots

As mentioned in Section 3.3, we will show the numerical results of Stokes problem for the offline GMsFEM using randomized snapshots. The convergence behaviors are shown in Tables 3 and 4 for perforated domain

DOF (# iter)	$\ e\ _{L^2}$	$\ e\ _{H^1}$
without adaptivity		
278	38.074	61.168
440 (1)	2.098	7.181
602 (2)	0.167	0.670
764 (3)	0.021	0.114
926 (4)	0.001	0.010
with adaptivity, $\eta_i^2 = r_i^2$		
278	38.074	61.168
436 (3)	1.058	4.493
628 (7)	0.029	0.175
760 (10)	0.002	0.014
950 (14)	5.339e-05	0.0003
with adaptivity, $\eta_i^2 = r_i^2 \lambda_{i+1}^{-1}$		
278	38.074	61.168
436 (3)	1.733	7.005
614 (7)	0.074	0.399
748 (10)	0.005	0.037
940 (14)	0.0002	0.001

DOF (# iter)	$\ e\ _{L^2}$	$\ e\ _{H^1}$
without adaptivity		
382	15.585	38.387
544 (1)	0.794	3.239
706 (2)	0.071	0.397
868 (3)	0.008	0.054
1030 (4)	0.0006	0.003
with adaptivity, $\eta_i^2 = r_i^2$		
382	15.585	38.387
556 (3)	0.477	2.116
704 (6)	0.033	0.211
892 (10)	0.001	0.007
1038 (13)	8.760e-05	0.0005
with adaptivity, $\eta_i^2 = r_i^2 \lambda_{i+1}^{-1}$		
382	15.585	38.387
548 (3)	0.528	2.377
740 (7)	0.019	0.124
878 (10)	0.001	0.010
1064 (14)	4.710e-05	0.0003

DOF (# iter)	$\ e\ _{L^2}$	$\ e\ _{H^1}$
without adaptivity		
648	8.870	27.343
810 (1)	0.611	2.390
972 (2)	0.063	0.376
1134 (3)	0.006	0.042
1296 (4)	0.0005	0.003
with adaptivity, $\eta_i^2 = r_i^2$		
648	8.870	27.343
820 (3)	0.301	1.400
972 (6)	0.021	0.140
1154 (10)	0.0006	0.004
1300 (13)	3.784e-05	0.0002
with adaptivity, $\eta_i^2 = r_i^2 \lambda_{i+1}^{-1}$		
648	8.870	27.343
810 (3)	0.309	1.500
996 (7)	0.008	0.067
1138 (10)	0.0006	0.005
1314 (14)	1.659e-05	0.0001

Table 2: Elasticity problem in the perforated domain with big inclusions (Figure 3, right). One (Left), Two (Middle) and Four (Right) offline basis functions ($\theta = 0.7$).

with small inclusions (Figure 3, left) and big inclusions (Figure 3, right), respectively, where the notation $\omega^{+, \epsilon} = \omega^\epsilon + 4$ means that the oversampled region $\omega^{+, \epsilon}$ is obtained by enlarging the region ω^ϵ by 4 fine grid cells. From these tables, we observe that the approach using randomized snapshots is more efficient since much fewer snapshot functions are used to achieve comparable accuracy. In particular, we get similar errors when the number of randomized snapshots is only around 20% of the number of standard snapshots. Notice that in the randomized snapshot construction, we need to add the constant basis, i.e., the constant function in each $\omega^{+, \epsilon}$. Note that, we do not have the constant basis in domain with inclusions when calculating snapshot basis in the standard way. This additional constant basis function makes the errors smaller for low degrees of freedom. For example, in the domain with small inclusions, when $DOF = 534$, the velocity L^2 error is 12.49% when we use standard snapshots, while the error is only 4.54% when the dimension of the randomized snapshots is 24.1% of the dimension of the whole snapshot space (see Table 3). However, when the DOF becomes larger, the errors for randomized snapshots are similar to that for standard snapshots. For instance, the velocity L^2 error is 0.07% when $DOF = 1986$ in domain with big inclusions for both standard snapshots and randomized snapshots (see Table 4), where the dimension of the randomized snapshot is 13.8% of the dimension of the whole snapshots. We remark that, by balancing the computational cost and accuracy, we find the results are satisfactory when 24.1% randomized snapshots for domain with small inclusions (Figure 3, left) and 20.7% randomized snapshots for domain with big inclusions (Figure 3, right) are used.

4.2.2 Adaptive online results

In this section, we present adaptive online results for Stokes problem for two perforated domains depicted in Figure 3. The solutions are shown in Figure 6 and Figure 7. In these figures, the x_1 -component and x_2 -component of the velocity solution are shown in the first and second rows, and the pressure solution is presented in the third row. The three columns contain the fine-scale, coarse-scale offline and coarse-scale online solutions. In both cases, we observe that the offline velocity solution is not able to capture the low values at the corners of the domain. Some features between inclusions also do not appear correctly in the

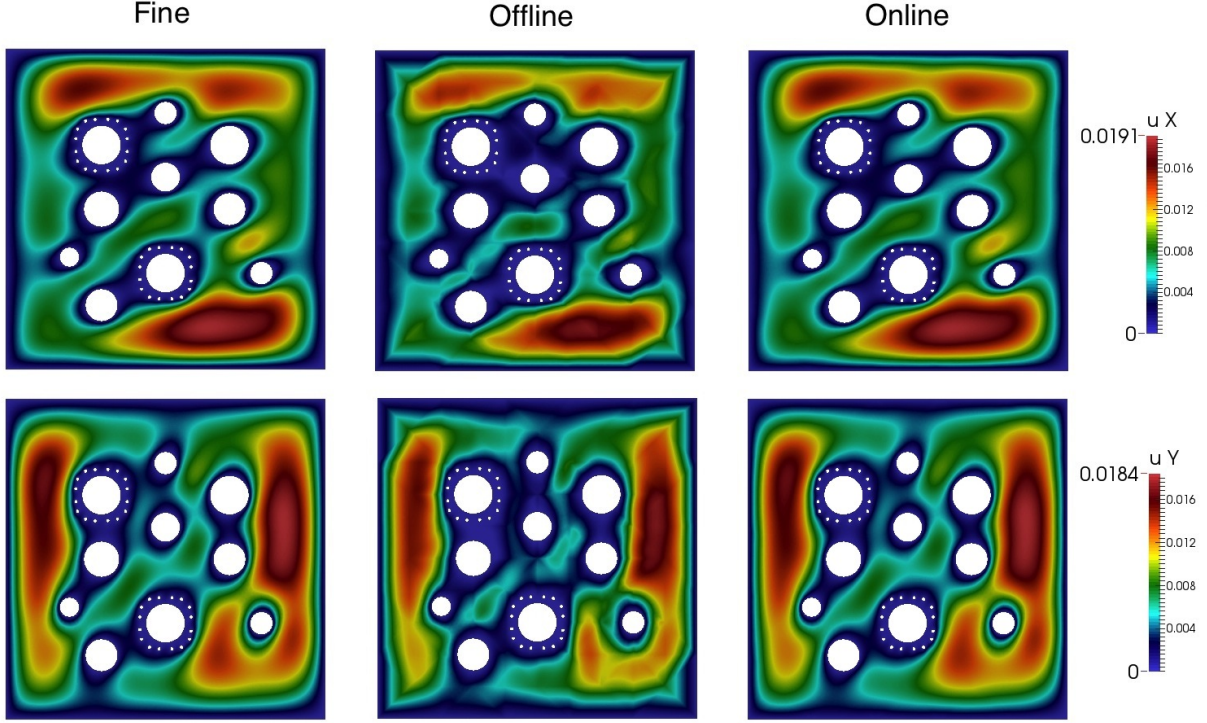


Figure 5: Elasticity problem in the perforated domain with big inclusions (Figure 3, right). Comparison of solutions in: Fine scale (left) $DOF = 21986$, Coarse scale offline, $DOF = 382$ (middle), Coarse scale online without adaptivity, $DOF = 544$ (right). Top: u_1 . Bottom: u_2 .

DOF	$\ \varepsilon_u\ _{L^2(\Omega)}(\%)$	$\ \varepsilon_u\ _{H^1(\Omega)}(\%)$	$\ \varepsilon_p\ _{L^2(\Omega)}(\%)$
Standard snapshot (100%)			
534	12.49	36.91	21.46
1018	0.28	4.67	0.86
1986	0.031	1.64	0.0029
Randomized snapshot: $\omega^{+, \epsilon} = \omega^\epsilon + 4$, 18.1%			
534	4.99	23.95	13.4
1018	0.54	7.05	0.53
1986	0.04	1.77	0.02
Randomized snapshot: $\omega^{+, \epsilon} = \omega^\epsilon + 4$, 24.1%			
534	4.54	22.69	8.28
1018	0.47	6.6	0.52
1986	0.036	1.72	0.009

Table 3: Perforated domain with small inclusions (Figure 3, left) for the Stokes problem using standard snapshots and randomized snapshots.

offline solution. For example, in Figure 6, the low values in the upper left and lower right corner of the domain are missing in the offline velocity solution. However, it was recovered very well in the online solution. Also, compared to the fine-scale solution, the features between the first hole on the left and the other inclusions are not captured in the offline solution. However, the online solutions get these features well and outputs

DOF	$\ \varepsilon_u\ _{L^2(\Omega)}(\%)$	$\ \varepsilon_u\ _{H^1(\Omega)}(\%)$	$\ \varepsilon_p\ _{L^2(\Omega)}(\%)$
Whole snapshot (100%)			
534	11.34	34.49	16.18
1018	0.17	3.62	1.09
1986	0.07	2.44	0.006
Randomized snapshot: $\omega^{+, \epsilon} = \omega^\epsilon + 4$, 13.8%			
534	6.04	24.84	9.37
1018	0.66	7.27	0.95
1986	0.07	2.53	0.02
Randomized snapshot: $\omega^{+, \epsilon} = \omega^\epsilon + 4$, 20.7%			
534	5.3	23.39	14.95
1018	0.56	6.87	0.73
1986	0.07	2.51	0.015

Table 4: Perforated domain with big inclusions (Figure 3, right) for the Stokes problem using standard snapshots and randomized snapshots.

almost same profiles as the fine solution. In Figure 7, for the domain has big inclusions with some extremely small inclusions around, we see even worse behavior of the offline solution compared to that in Figure 6, where the domain has several small inclusions. The low values of the velocity solution in the x_2 -component along the right boundary are almost missing in the offline solution. The offline velocity solutions in both components around inclusions are still very poor. These observations highlights the advantage of the online method. We performed other tests for different perforated domains, and the results also suggest that online method is quite necessary.

Now, we turn our attention to velocity $L^2(\Omega^\epsilon)$, $H^1(\Omega^\epsilon)$ errors and pressure $L^2(\Omega^\epsilon)$ error presented in Table 5 and Table 6. We consider different numbers of initial basis on each coarse neighborhood. For the perforated domain with small inclusions in Figure 6, we observe from Table 5 that both the velocity and pressure error decrease faster as we choose more initial bases. For example, the velocity has large H^1 error 66.28% using one initial basis. After adding one online basis, it reduces to 22.3%. When two initial bases are selected, the velocity H^1 error reduces from 23.4% to 3.2% after one step enrichment. Fixing the number of initial basis, we can compare the error behavior for the online method with or without adaptivity. It appears that online adaptive method reduces the errors more effectively. For instance, when one initial basis is selected, the velocity H^1 error is 22.302% for DOF 488 using non-adaptive online algorithm, while it is only 3.067% for a similar DOF 499 using adaptive online method with indicator 1 (see (16)). Comparing two error indicators for adaptive online method, we see that the indicator 1 is preferred when choosing one initial basis. Since the velocity error is 8.758% for DOF 504 using indicator 2 (see (17)), which is much larger than 3.067%. Also, the pressure error is 16.559% in this case when using indicator 2, which is almost 5 times larger compared with 3.575% when using indicator 1. However, both indicator works well when selecting more initial bases. We see very similar errors for both velocity and pressure fields using different indicators when the number of initial basis is two or three.

For the second example in Figure 7, results are shown in Table 6. In this case, we observe that the online approach works better if we start with more initial basis. For example, the velocity H^1 error is 71.823% with one initial velocity basis, and reduces to 24.460% after adding one online basis. However it's only 20.430% with two initial basis without online enrichment. This implies that it is better to start with two or more initial basis in order to see that the more the online basis are used, the smaller the errors become. Similarly as before, the online approach with the adaptivity reduces the errors faster. Compared the two indicators, we see that the first error indicator (see (16)) for the adaptive online method gives slightly better results for any number of initial basis. One can also find that the pressure error also reduces significantly when we only enrich the velocity space.

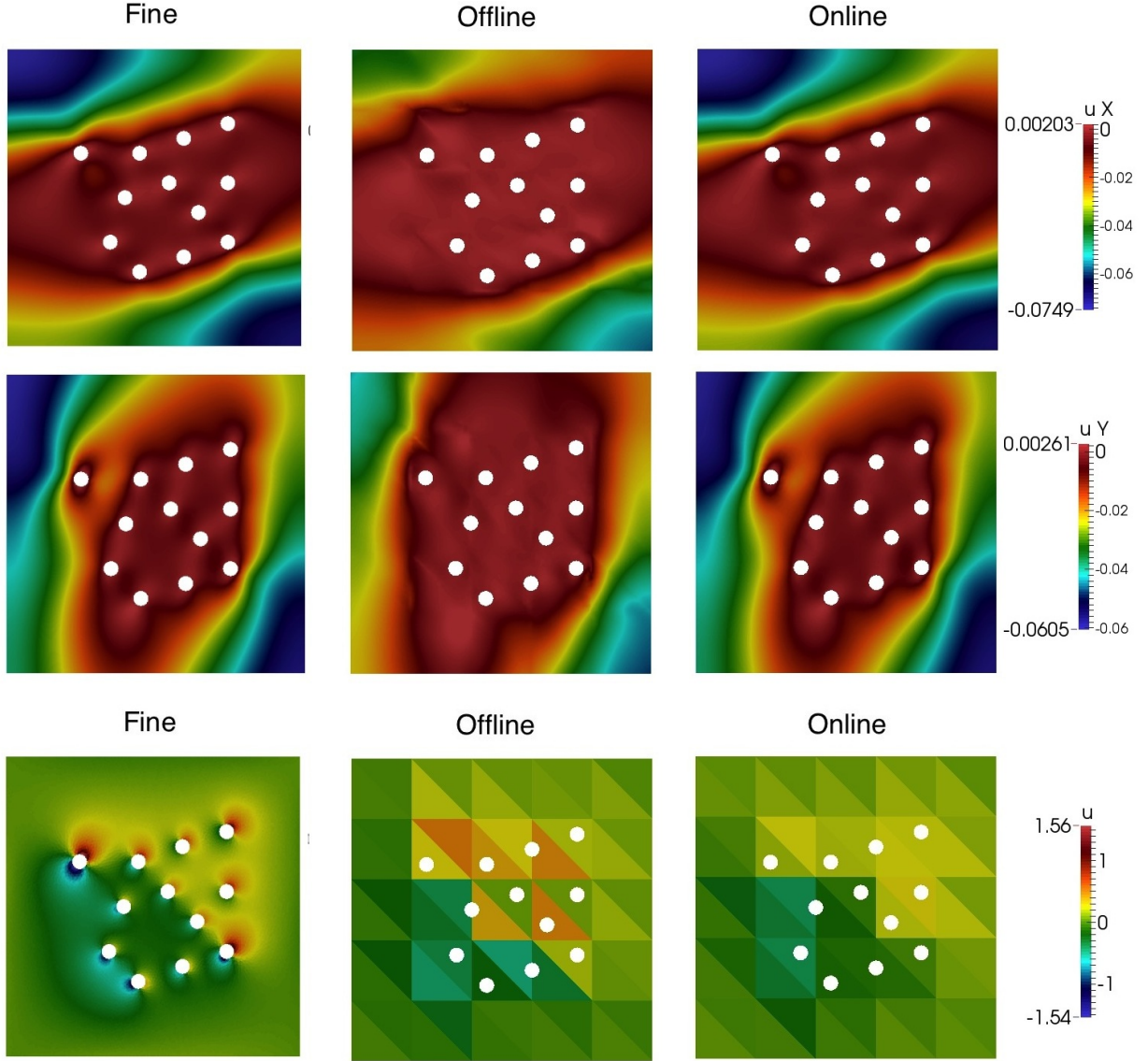


Figure 6: Stokes problem. Fine-scale and multiscale solutions for velocity and pressure (u_1 (Top), u_2 (Middle) and p (Bottom)) in perforated domain with small inclusions (Figure 3, left). Left: fine-scale solution, $DOF = 77524$. Middle: multiscale solutions using 1 multiscale basis function for velocity, $DOF = 452$, velocity L^2 error is 42.439 %. Right: multiscale solutions after 2 online iteration without adaptivity, $DOF = 524$, velocity L^2 error is 1.688 %.

5 Convergence Analysis

The result in [16] has shown the convergence for online adaptive method applied to elliptic problems, and the same results can be applied for elasticity problem. In this section, we will prove the convergence of adaptive online GMsFEM for Stokes problem.

First, we will prove the following inf-sup condition for the approximation of Stokes problem using offline

DOF (# iter)	$\ e_u\ _{L^2}(\%)$	$\ e_u\ _{H^1}(\%)$	$\ e_{\bar{p}}\ _{L^2}(\%)$
452	42.439	66.276	81.954
without adaptivity			
488 (1)	6.300	22.302	41.776
524 (2)	1.688	7.191	10.376
596 (4)	0.111	0.692	0.809
740 (8)	0.042	0.514	0.036
with adaptivity, $\eta_i^2 = r_i^2$			
499 (4)	0.627	3.067	3.575
532 (6)	0.074	0.772	0.329
596 (10)	0.042	0.515	0.038
723 (20)	0.033	0.411	0.146
with adaptivity, $\eta_i^2 = r_i^2 \lambda_{i+1}^{-1}$			
504 (3)	1.397	8.758	16.559
546 (5)	0.411	2.617	3.594
611 (8)	0.089	0.709	0.482
750 (15)	0.042	0.517	0.036

DOF (# iter)	$\ e_u\ _{L^2}(\%)$	$\ e_u\ _{H^1}(\%)$	$\ e_{\bar{p}}\ _{L^2}(\%)$
694	5.467	23.329	13.775
without adaptivity			
730 (1)	0.400	3.212	1.187
766 (2)	0.066	1.137	0.135
838 (4)	0.033	0.614	0.053
982 (8)	0.011	0.216	0.016
with adaptivity, $\eta_i^2 = r_i^2$			
732 (3)	0.093	1.335	0.227
781 (6)	0.041	0.742	0.079
844 (10)	0.019	0.367	0.021
992 (20)	0.004	0.104	0.003
with adaptivity, $\eta_i^2 = r_i^2 \lambda_{i+1}^{-1}$			
745 (2)	0.088	1.362	0.310
769 (3)	0.057	0.982	0.110
841 (6)	0.030	0.562	0.026
988 (12)	0.011	0.216	0.022

DOF (# iter)	$\ e_u\ _{L^2}(\%)$	$\ e_u\ _{H^1}(\%)$	$\ e_{\bar{p}}\ _{L^2}(\%)$
936	0.936	8.795	8.515
without adaptivity			
972 (1)	0.032	0.782	0.118
1008 (2)	0.013	0.445	0.018
1080 (4)	0.007	0.261	0.005
1224 (8)	0.003	0.106	0.001
with adaptivity, $\eta_i^2 = r_i^2$			
975 (3)	0.016	0.493	0.026
1011 (6)	0.009	0.311	0.007
1082 (10)	0.005	0.167	0.003
1227 (20)	0.002	0.078	0.001
with adaptivity, $\eta_i^2 = r_i^2 \lambda_{i+1}^{-1}$			
1003 (2)	0.013	0.449	0.018
1037 (3)	0.010	0.343	0.007
1105 (5)	0.006	0.218	0.004
1241 (9)	0.002	0.094	0.001

Table 5: Stokes problem for perforated domain with small inclusions(Figure 3, left). One (Upper left), Two (Upper right) and Three e(Bottom) offline basis functions ($\theta = 0.7$).

GMsFEM. This ensures that the method, with both offline and online basis functions, is well-posed. We will assume the continuous inf-sup condition holds. In particular, there is a constant $C_{\text{cont}} > 0$ such that for any $p \in L^2(\Omega^\epsilon)$ with zero mean, we have

$$\sup_{v \in (H_0^1(\Omega^\epsilon))^2} \frac{\int_{\Omega^\epsilon} \text{div}(v)p}{\|v\|_{H^1(\Omega^\epsilon)}} \geq C_{\text{cont}} \|p\|_{L^2(\Omega^\epsilon)}. \quad (26)$$

Equivalently, there exists $v \in (H_0^1(\Omega^\epsilon))^2$ such that $\text{div } v = p$ and $\|v\|_{H^1(\Omega^\epsilon)} \leq C_{\text{cont}}^{-1} \|p\|_{L^2(\Omega^\epsilon)}$. Let N_e^0 be the number of interior coarse edges. We remark that, for each interior coarse edge E_i , there exists a basis function Φ_i^{off} such that $\int_{E_i} \Phi_i^{\text{off}} \cdot n_i \neq 0$.

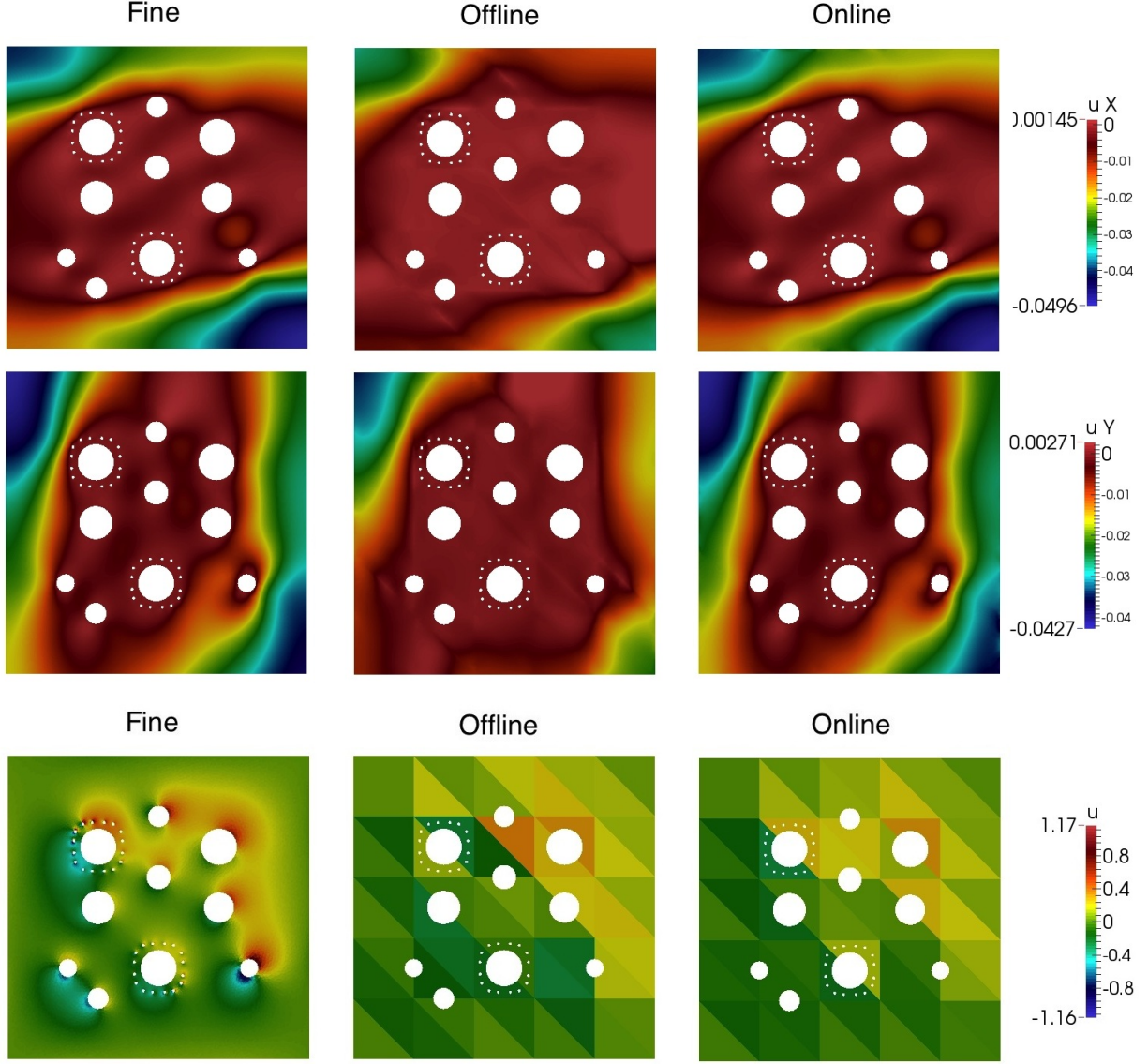


Figure 7: Stokes problem. Fine-scale and multiscale solutions for velocity and pressure (u_1 (Top), u_2 (Middle) and p (Bottom)) in perforated domain with big inclusions(Figure 3, right). Left: fine-scale solution, $DOF = 101386$. Middle: multiscale solutions using 1 multiscale basis function for velocity, $DOF = 452$, velocity L^2 error is 47.943 %. Right: multiscale solutions after 2 online iteration without adaptivity, $DOF = 524$, velocity L^2 error is 2.266 %.

Lemma 5.1. *For all $p \in Q_{\text{off}}$, there is a constant $C_{\text{infsup}} > 0$ such that*

$$\sup_{u \in V_{\text{off}}} \frac{\int_{\Omega^\epsilon} \text{div}(u)p}{\|u\|_{H^1(\Omega^\epsilon)}} \geq C_{\text{infsup}} \|p\|_{L^2(\Omega^\epsilon)}. \quad (27)$$

Proof. Let $p \in Q_{\text{off}}$ with zero mean. Using the continuous inf-sup condition (26), there exists $v \in H_0^1(\Omega^\epsilon)$ such that $\text{div } v = p$ and $\|v\|_{H^1(\Omega^\epsilon)} \leq C_{\text{cont}}^{-1} \|p\|_{L^2(\Omega^\epsilon)}$. Since, for each interior coarse edge E_i , there exists a

DOF (# iter)	$\ e_u\ _{L^2}(\%)$	$\ e_u\ _{H^1}(\%)$	$\ e_{\bar{p}}\ _{L^2}(\%)$
452	47.943	71.823	88.414
without adaptivity			
488 (1)	8.039	24.460	21.206
524 (2)	2.266	12.286	11.107
596 (4)	0.419	2.477	1.433
740 (8)	0.050	0.733	0.038
with adaptivity, $\eta_i^2 = r_i^2$			
492 (3)	2.444	13.528	11.355
534 (6)	0.546	4.315	3.168
593 (10)	0.087	0.870	0.282
718 (20)	0.041	0.501	0.025
with adaptivity, $\eta_i^2 = r_i^2 \lambda_{i+1}^{-1}$			
511 (2)	2.346	12.396	10.890
543 (3)	1.302	7.944	3.784
605 (5)	0.175	1.157	0.443
768 (11)	0.043	0.507	0.068

DOF (# iter)	$\ e_u\ _{L^2}(\%)$	$\ e_u\ _{H^1}(\%)$	$\ e_{\bar{p}}\ _{L^2}(\%)$
694	4.117	20.430	13.635
without adaptivity			
730 (1)	0.260	2.293	1.443
766 (2)	0.075	0.982	0.057
838 (4)	0.030	0.469	0.030
982 (8)	0.008	0.169	0.005
with adaptivity, $\eta_i^2 = r_i^2$			
735 (3)	0.085	1.100	0.070
766 (5)	0.049	0.678	0.031
842 (10)	0.016	0.254	0.023
981 (20)	0.006	0.133	0.002
with adaptivity, $\eta_i^2 = r_i^2 \lambda_{i+1}^{-1}$			
762 (2)	0.075	0.982	0.057
796 (3)	0.055	0.776	0.056
864 (5)	0.024	0.388	0.014
1000 (9)	0.007	0.149	0.004

DOF (# iter)	$\ e_u\ _{L^2}(\%)$	$\ e_u\ _{H^1}(\%)$	$\ e_{\bar{p}}\ _{L^2}(\%)$
936	0.407	5.627	2.091
without adaptivity			
972 (1)	0.030	0.720	0.058
1008 (2)	0.019	0.490	0.014
1080 (4)	0.007	0.197	0.004
1224 (8)	0.004	0.119	0.002
with adaptivity, $\eta_i^2 = r_i^2$			
977 (3)	0.022	0.564	0.027
1023 (6)	0.010	0.275	0.011
1085 (10)	0.006	0.167	0.003
1226 (19)	0.003	0.089	0.001
with adaptivity, $\eta_i^2 = r_i^2 \lambda_{i+1}^{-1}$			
972 (1)	0.030	0.720	0.058
1040 (3)	0.012	0.303	0.009
1108 (5)	0.006	0.161	0.003
1244 (9)	0.003	0.092	0.002

Table 6: Stokes problem for perforated domain with big inclusions(Figure 3, right). One (Upper left), Two (Upper right) and Three (Bottom) offline basis functions ($\theta = 0.7$).

basis function Φ_i^{off} such that $\int_{E_i} \Phi_i^{\text{off}} \cdot n_i \neq 0$. We can then define $u \in V_{\text{off}}$ by the following

$$u = \sum_{i=1}^{N_e^0} c_i \Phi_i^{\text{off}}, \quad c_i = \int_{E_i} v \cdot n_i$$

where we assume that the basis function are normalized so that $\int_{E_i} \Phi_i^{\text{off}} \cdot n_i = 1$. So, by the Green's identity, we have

$$\int_{\Omega^\epsilon} p^2 = \int_{\Omega^\epsilon} \text{div}(v)p = \sum_{i=1}^{N_e^0} \int_{E_i} (v \cdot n_i)[p] = \sum_{i=1}^{N_e^0} \int_{E_i} c_i (\Phi_i^{\text{off}} \cdot n_i)[p] = \int_{\Omega^\epsilon} \text{div}(u)p$$

where $[p]$ is the jump of p . We will next show that there is a constant $C_{\text{inf-sup}} > 0$ such that $\|u\|_{H^1(\Omega^\epsilon)} \leq C_{\text{inf-sup}}^{-1} \|p\|_{L^2(\Omega^\epsilon)}$.

Since $c_i^2 \leq H \int_{E_i} (v \cdot n_i)^2$, we have

$$\|\nabla u\|_{L^2(\Omega^\epsilon)}^2 \leq \sum_{i=1}^{N_e^0} \int_{\omega_i^\epsilon} c_i^2 \nabla \Phi_i^{\text{off}} : \nabla \Phi_i^{\text{off}} \leq C_{\text{max}} H \sum_{K \in \mathcal{T}^H} \int_{\partial K} (v \cdot n)^2$$

where $C_{\text{max}} = \max_{1 \leq i \leq N_e^0} C_i$ and $C_i = \min \int_{\omega_i^\epsilon} \nabla \Phi_i^{\text{off}} : \nabla \Phi_i^{\text{off}}$ with the minimum taken over all basis functions Φ_i^{off} such that $\int_{E_i} \Phi_i^{\text{off}} \cdot n_i \neq 0$. Notice that the constant C_i are independent of the mesh size. Using the trace theorem on the coarse element K , we have $H \int_{\partial K} (v \cdot n)^2 \preceq \|v\|_{H^1(K)}^2$. So, by the continuous inf-sup condition, we obtain

$$\sum_{K \in \mathcal{T}^H} H \int_{\partial K} (v \cdot n)^2 \preceq \|v\|_{H^1(\Omega^\epsilon)}^2 \preceq \|p\|_{L^2(\Omega^\epsilon)}^2.$$

This completes the proof. \square

Now, we will show the convergence of our online adaptive enrichment scheme for the Stokes problem. First, we define a reference solution by $(u, p) \in (H_0^1(\Omega^\epsilon))^2 \times Q_{\text{off}}$ which solves

$$\langle \mathcal{L}^\epsilon(u, p), (v, q) \rangle_{\Omega^\epsilon} = ((f, 0), (v, q))_{\Omega^\epsilon}, \quad \text{for all } (v, q) \in H_0^1(\Omega^\epsilon)^2 \times Q_{\text{off}}. \quad (28)$$

Notice that the solution of (28) and the solution of (10) have a difference proportional to the coarse mesh size H . We also define a snapshot solution by $(\hat{u}, \hat{p}) \in V_{\text{snap}} \times Q_{\text{off}}$ which solves

$$\langle \mathcal{L}^\epsilon(\hat{u}, \hat{p}), (v, q) \rangle_{\Omega^\epsilon} = ((f, 0), (v, q))_{\Omega^\epsilon}, \quad \text{for all } (v, q) \in V_{\text{snap}} \times Q_{\text{off}}. \quad (29)$$

We notice that the difference $\|u - \hat{u}\|_{H^1(\Omega^\epsilon)}$ represents an irreducible error. Furthermore, standard finite element analysis shows that

$$\|u - u_{\text{ms}}\|_{H^1(\Omega^\epsilon)} \leq \|u - \tilde{u}_{\text{ms}}\|_{H^1(\Omega^\epsilon)} \quad (30)$$

for any $\tilde{u}_{\text{ms}} \in V_{\text{off}}$. Next, we prove the following a-posteriori error bound for the offline GMsFEM (11). The notation $a \preceq b$ means that there is a generic constant $C > 0$ such that $a \leq Cb$.

Theorem 5.2. *Let u be the reference solution defined in (28), \hat{u} be the snapshot solution defined in (29) and u_{ms} be the multiscale solution satisfying (11). Then, we have*

$$\|\hat{u} - u_{\text{ms}}\|_{H^1(\Omega^\epsilon)}^2 \leq C_s \sum_{i=1}^{N_u} \left(1 + \frac{1}{\lambda_{l_i+1}^{i, \text{off}}}\right) \|R_i\|_{V^*}^2 \quad (31)$$

where l_i is the number of offline basis functions used for the coarse neighborhood ω_i^ϵ , and $\lambda_j^{i, \text{off}}$ is the j -th eigenvalue for the coarse neighborhood ω_i^ϵ . The constant C_s is the maximum number of coarse neighborhoods corresponding to coarse blocks. Moreover, we have

$$\|u - u_{\text{ms}}\|_{H^1(\Omega^\epsilon)}^2 \leq 2C_s \sum_{i=1}^{N_u} \left(1 + \frac{1}{\lambda_{l_i+1}^{i, \text{off}}}\right) \|R_i\|_{V^*}^2 + 2\|u - \hat{u}\|_{H^1(\Omega^\epsilon)}^2. \quad (32)$$

Proof. For any $\phi \in V_{\text{snap}}$ such that $\int_{K_i^\epsilon} \text{div } \phi = 0$ and $\phi = \mathcal{H}(\phi)$, we have

$$\int_{\Omega^\epsilon} \nabla(\hat{u} - u_{\text{ms}}) : \nabla \phi = \int_{\Omega^\epsilon} \nabla(\hat{u} - u_{\text{ms}}) : \nabla \phi - \int_{\Omega^\epsilon} (\hat{p} - p_{\text{ms}}) \text{div } \phi \quad (33)$$

where we use the fact that $\int_{K_i^\epsilon} (\hat{p} - p_{\text{ms}}) \operatorname{div} \phi = 0$ since $\hat{p} - p_{\text{ms}}$ is constant in K_i^ϵ . We can write (33) as

$$\int_{\Omega^\epsilon} \nabla(\hat{u} - u_{\text{ms}}) : \nabla \phi = R(\phi) \quad (34)$$

where $R(\phi)$ is the global residual defined by $R(\phi) = \int_{\Omega^\epsilon} \nabla(u - u_{\text{ms}}) : \nabla \phi - \int_{\Omega^\epsilon} (p - p_{\text{ms}}) \operatorname{div} \phi$ for all ϕ . Let ϕ^{off} be an arbitrary function in the space V_{off} . We can write $\phi^{\text{off}} = \sum_{i=1}^{N_u} \phi_i^{\text{off}}$ where ϕ_i^{off} is the component of ϕ^{off} in the local offline space corresponding to the coarse neighborhood ω_i^ϵ . Using the facts that $V_{\text{off}} \subset V_{\text{snap}}$ and $R(\phi^{\text{off}}) = 0$, we can write $R(\phi)$ as

$$R(\phi) = R(\mathcal{H}(\phi) - \phi^{\text{off}}) = R\left(\sum_{i=1}^{N_u} (\mathcal{H}(\chi_i \phi) - \phi_i^{\text{off}})\right) = \sum_{i=1}^{N_u} R_i(\mathcal{H}(\chi_i \phi) - \phi_i^{\text{off}}) \quad (35)$$

where R_i is the local residual defined in (23). We will define ϕ^{off} as follows. Notice that $\mathcal{H}(\chi_i \phi)$ belongs to the local snapshot space V_{snap}^i . We can take ϕ_i^{off} as the component of $\mathcal{H}(\chi_i \phi)$ in the offline space V_{off}^i . We write $\phi_i^{\text{off}} = \mathcal{H}(\chi_i \phi_i)$.

Then from (35), we have

$$R(\phi) \leq \sum_{i=1}^{N_u} \|R_i\|_{(V^i)^*} \|\mathcal{H}(\chi_i \phi) - \mathcal{H}(\chi_i \phi_i)\|_{H^1(\omega_i^\epsilon)}.$$

Using the minimum energy property, we have

$$R(\phi) \leq \sum_{i=1}^{N_u} \|R_i\|_{(V^i)^*} \|\chi_i(\phi - \phi_i)\|_{H^1(\omega_i^\epsilon)}.$$

By the spectral problem (19), we obtain

$$R(\phi) \leq \sum_{i=1}^{N_u} \left(1 + \frac{1}{\lambda_{l_i+1}^{i,\text{off}}}\right)^{\frac{1}{2}} \|R_i\|_{(V^i)^*} \|\phi - \phi_i\|_{H^1(\omega_i^\epsilon)} \leq \sum_{i=1}^{N_u} \left(1 + \frac{1}{\lambda_{l_i+1}^{i,\text{off}}}\right)^{\frac{1}{2}} \|R_i\|_{(V^i)^*} \|\phi\|_{H^1(\omega_i^\epsilon)} \quad (36)$$

where we used the orthogonality of eigenfunctions from the spectral problem (19). Finally, we take $\phi = \hat{u} - u_{\text{ms}}$. Notice that, by (29) and (11), we have

$$\int_{K_i^\epsilon} \operatorname{div}(\hat{u} - u_{\text{ms}}) = 0.$$

In addition, for this choice of ϕ , we have $\phi = \mathcal{H}(\phi)$ since $\hat{u}, u_{\text{ms}} \in V_{\text{snap}}$. Hence (34) and (36) imply that

$$\|\hat{u} - u_{\text{ms}}\|_{H^1(\Omega^\epsilon)}^2 \leq \sum_{i=1}^{N_u} \left(1 + \frac{1}{\lambda_{l_i+1}^{i,\text{off}}}\right)^{\frac{1}{2}} \|R_i\|_{(V^i)^*} \|\hat{u} - u_{\text{ms}}\|_{H^1(\omega_i^\epsilon)},$$

which shows (31). The proof for (32) follows from $\|u - u_{\text{ms}}\|_{H^1(\Omega^\epsilon)} \leq \|u - \hat{u}\|_{H^1(\Omega^\epsilon)} + \|\hat{u} - u_{\text{ms}}\|_{H^1(\Omega^\epsilon)}$. \square

We recall that the norm of the local residual R_i is defined in (24). We define a modified norm as

$$\|R_i\|_{(V_0^i)^*} = \sup_{v \in V_0^i} \frac{|R_i(v)|}{\|v\|_{H^1(\omega_i^\epsilon)}} \quad (37)$$

where $V_0^i \subset V^i$ and the vectors $v \in V_0^i$ satisfies $\int_{\Omega^\epsilon} \operatorname{div}(v) q = 0$ for all $q \in Q_{\text{off}}$. It is easy to show that $\|R_i\|_{(V_0^i)^*} \leq \|R_i\|_{(V^i)^*}$. In the next theorem, we will show the convergence of the online adaptive GMSFEM for the Stokes problem. The theorem states that our method is convergent up to an irreducible error $\|u - \hat{u}\|_{H^1(\Omega^\epsilon)}$ with enough number of offline basis functions.

Theorem 5.3. *Let u be the reference solution defined in (28), \hat{u} be the snapshot solution defined in (29) and u_{ms}^m be the multiscale solution of (11) in the enrichment level m . Assume that l_i offline basis functions for the coarse neighborhood ω_i^ϵ are used as initial basis in the online procedure. Suppose that one online basis is added to a single coarse neighborhood ω_i^ϵ . Then, there is a constant D such that*

$$\|u - u_{\text{ms}}^{m+1}\|_{H^1(\Omega^\epsilon)}^2 \leq (1 + \delta_3)(1 + \delta_2) \left(1 + \delta_1 - \theta C_s^{-1} \frac{\lambda_{l_i+1}^{i,\text{off}}}{\lambda_{l_i+1}^{i,\text{off}} + 1} \right) \|\hat{u} - u_{\text{ms}}^m\|_{H^1(\Omega^\epsilon)}^2 + D \|u - \hat{u}\|_{H^1(\Omega^\epsilon)}^2 \quad (38)$$

where $\delta_1, \delta_2, \delta_3 > 0$ are arbitrary and D depends only on $\delta_i, i = 1, 2, 3$. In addition, θ is the relative residual defined by

$$\theta = \|R_i\|_{(V_0^i)^*}^2 / \sum_{i=1}^{N_u} \|R_i\|_{(V^i)^*}^2.$$

Proof. We will first consider the addition of only one online basis function ϕ_i^{on} to the space V_{off}^m . For any function $\tilde{u}_{\text{ms}} \in V_{\text{off}}^{m+1}$, by (30), we have

$$\|u - u_{\text{ms}}^{m+1}\|_{H^1(\Omega^\epsilon)} \leq \|u - \tilde{u}_{\text{ms}}\|_{H^1(\Omega^\epsilon)} \leq \|\hat{u} - \tilde{u}_{\text{ms}}\|_{H^1(\Omega^\epsilon)} + \|u - \hat{u}\|_{H^1(\Omega^\epsilon)}. \quad (39)$$

We will derive an estimate for $\|\hat{u} - \tilde{u}_{\text{ms}}\|_{H^1(\Omega^\epsilon)}$. We take $\tilde{u}_{\text{ms}} = u_{\text{ms}}^m + \alpha \phi_i^{\text{on}}$ where α is a scalar to be determined. Then we have

$$\|\hat{u} - \tilde{u}_{\text{ms}}\|_{H^1(\Omega^\epsilon)}^2 = \|\hat{u} - u_{\text{ms}}^m\|_{H^1(\Omega^\epsilon)}^2 - 2\alpha \int_{\omega_i^\epsilon} \nabla(\hat{u} - u_{\text{ms}}^m) : \nabla \phi_i^{\text{on}} + \alpha^2 \|\phi_i^{\text{on}}\|_{H^1(\Omega^\epsilon)}^2.$$

Using the definition of the residual R_i and the fact that $\int_{\omega_i^\epsilon} \text{div}(\phi_i^{\text{on}}) q = 0$ for all $q \in Q_{\text{off}}$, we have

$$\|\hat{u} - \tilde{u}_{\text{ms}}\|_{H^1(\Omega^\epsilon)}^2 = \|\hat{u} - u_{\text{ms}}^m\|_{H^1(\Omega^\epsilon)}^2 - 2\alpha R_i(\phi_i^{\text{on}}) + \alpha^2 \|\phi_i^{\text{on}}\|_{H^1(\Omega^\epsilon)}^2 + 2\alpha \int_{\omega_i^\epsilon} \nabla(u - \hat{u}) : \nabla \phi_i^{\text{on}}.$$

Taking $\alpha = R_i(\phi_i^{\text{on}}) / \|\phi_i^{\text{on}}\|_{H^1(\omega_i^\epsilon)}^2$, we have

$$\|\hat{u} - \tilde{u}_{\text{ms}}\|_{H^1(\Omega^\epsilon)}^2 = \|\hat{u} - u_{\text{ms}}^m\|_{H^1(\Omega^\epsilon)}^2 - \frac{R_i(\phi_i^{\text{on}})^2}{\|\phi_i^{\text{on}}\|_{H^1(\omega_i^\epsilon)}^2} + 2\alpha \int_{\omega_i^\epsilon} \nabla(u - \hat{u}) : \nabla \phi_i^{\text{on}}. \quad (40)$$

Using (25), we have

$$R_i(v) = \int_{\omega_i^\epsilon} \nabla \phi_i^{\text{on}} : \nabla v, \quad \forall v \in V_0^i. \quad (41)$$

By (37) and (41), we have $\|R_i\|_{(V_0^i)^*} \leq \|\phi_i^{\text{on}}\|_{H^1(\omega_i^\epsilon)}$. Taking $v = \phi_i^{\text{on}}$ in (41), we have $R_i(\phi_i^{\text{on}}) = \|\phi_i^{\text{on}}\|_{H^1(\omega_i^\epsilon)}^2$. Thus, (40) becomes

$$\|\hat{u} - \tilde{u}_{\text{ms}}\|_{H^1(\Omega^\epsilon)}^2 = \|\hat{u} - u_{\text{ms}}^m\|_{H^1(\Omega^\epsilon)}^2 - \|R_i\|_{(V_0^i)^*}^2 + 2\alpha \int_{\omega_i^\epsilon} \nabla(u - \hat{u}) : \nabla \phi_i^{\text{on}}. \quad (42)$$

Using the definition of θ and (31), we have

$$\|\hat{u} - \tilde{u}_{\text{ms}}\|_{H^1(\Omega^\epsilon)}^2 \leq \left(1 - \theta C_s^{-1} \frac{\lambda_{l_i+1}^{i,\text{off}}}{\lambda_{l_i+1}^{i,\text{off}} + 1} \right) \|\hat{u} - u_{\text{ms}}^m\|_{H^1(\Omega^\epsilon)}^2 + 2\alpha \int_{\omega_i^\epsilon} \nabla(u - \hat{u}) : \nabla \phi_i^{\text{on}}. \quad (43)$$

The last term in (43) can be estimated as

$$2\alpha \int_{\omega_i^\epsilon} \nabla(u - \hat{u}) : \nabla \phi_i^{\text{on}} \leq 2\|u - \hat{u}\|_{H^1(\Omega^\epsilon)} \frac{R_i(\phi_i^{\text{on}})}{\|\phi_i^{\text{on}}\|_{H^1(\omega_i^\epsilon)}}$$

Using the definition of R_i , we have $R_i(\phi_i^{\text{on}}) = \int_{\omega_i^\epsilon} \nabla(u - u_{\text{ms}}^m) : \nabla \phi_i^{\text{on}}$. So,

$$2\alpha \int_{\omega_i^\epsilon} \nabla(u - \hat{u}) : \nabla \phi_i^{\text{on}} \leq 2\|u - \hat{u}\|_{H^1(\Omega^\epsilon)} \|u - u_{\text{ms}}^m\|_{H^1(\Omega^\epsilon)}.$$

Notice that $2\|u - \hat{u}\|_{H^1(\Omega^\epsilon)} \|\hat{u} - u_{\text{ms}}^m\|_{H^1(\Omega^\epsilon)} \leq \delta_1^{-1} \|u - \hat{u}\|_{H^1(\Omega^\epsilon)}^2 + \delta_1 \|\hat{u} - u_{\text{ms}}^m\|_{H^1(\Omega^\epsilon)}^2$ for any $\delta_1 > 0$. Therefore, (43) becomes

$$\|\hat{u} - \tilde{u}_{\text{ms}}\|_{H^1(\Omega^\epsilon)}^2 \leq \left(1 + \delta_1 - \theta C_s^{-1} \frac{\lambda_{l_i+1}^{i,\text{off}}}{\lambda_{l_i+1}^{i,\text{off}} + 1}\right) \|\hat{u} - u_{\text{ms}}^m\|_{H^1(\Omega^\epsilon)}^2 + (2 + \delta_1^{-1}) \|u - \hat{u}\|_{H^1(\Omega^\epsilon)}^2. \quad (44)$$

Finally, combining (39) and (44), we have

$$\|u - u_{\text{ms}}^{m+1}\|_{H^1(\Omega^\epsilon)}^2 \leq (1 + \delta_2) \left(1 + \delta_1 - \theta C_s^{-1} \frac{\lambda_{l_i+1}^{i,\text{off}}}{\lambda_{l_i+1}^{i,\text{off}} + 1}\right) \|\hat{u} - u_{\text{ms}}^m\|_{H^1(\Omega^\epsilon)}^2 + (3 + \delta_1^{-1} + \delta_2^{-1}) \|u - \hat{u}\|_{H^1(\Omega^\epsilon)}^2. \quad (45)$$

We obtain the desired result by noting that

$$\|\hat{u} - u_{\text{ms}}^m\|_{H^1(\Omega^\epsilon)}^2 \leq (1 + \delta_3) \|u - u_{\text{ms}}^m\|_{H^1(\Omega^\epsilon)}^2 + (1 + \delta_3^{-1}) \|u - \hat{u}\|_{H^1(\Omega^\epsilon)}^2$$

for any $\delta_3 > 0$. □

We remark that, in order to obtain rapid convergence, one needs to choose l_i large enough so that $\lambda_{l_i+1}^{i,\text{off}}$ is large. In this case, the quantity $\lambda_{l_i+1}^{i,\text{off}}/(\lambda_{l_i+1}^{i,\text{off}} + 1)$ is close to one. Then, (38) shows that the resulting online adaptive enrichment procedure has a rapid convergence.

Theorem 5.3 gives the convergence of our online adaptive enrichment procedure when one online basis is added at a time. One can also add online basis in non-overlapping coarse neighborhoods. Using the same proof as Theorem 5.3, we obtain the following result.

Theorem 5.4. *Let u be the reference solution defined in (28), \hat{u} be the snapshot solution defined in (29) and u_{ms}^m be the multiscale solution of (11) in the enrichment level m . Assume that l_i offline basis functions for the coarse neighborhood ω_i^ϵ are used as initial basis in the online procedure. Let S be the index set for the non-overlapping coarse neighborhoods where online basis functions are added. Then, there is a constant D such that*

$$\|u - u_{\text{ms}}^{m+1}\|_{H^1(\Omega^\epsilon)}^2 \leq (1 + \delta_3)(1 + \delta_2) \left(1 + \delta_1 - \theta C_s^{-1} \min_{j \in S} \frac{\lambda_{l_j+1}^{i,\text{off}}}{\lambda_{l_j+1}^{i,\text{off}} + 1}\right) \|\hat{u} - u_{\text{ms}}^m\|_{H^1(\Omega^\epsilon)}^2 + D \|u - \hat{u}\|_{H^1(\Omega^\epsilon)}^2 \quad (46)$$

where $\delta_1, \delta_2, \delta_3 > 0$ are arbitrary and D depends only on $\delta_i, i = 1, 2, 3$. In addition, θ is the relative residual defined by

$$\theta = \sum_{i \in S} \|R_i\|_{(V_0^i)^*}^2 / \sum_{i=1}^{N_u} \|R_i\|_{(V^i)^*}^2.$$

The above result suggests that adding more online basis functions at each iteration will speed up the convergence. Lastly, we remark that the convergence for the pressure can be obtained using the inf-sup condition (27).

6 Conclusion

We present an efficient multiscale procedure for solving PDEs in perforated domains. We consider elliptic, elastic, and Stokes systems. In our previous work [18], we presented a first step in constructing the offline multiscale basis functions (without analysis) for solving PDEs in perforated domains. It is known that the convergence of multiscale methods can be significantly accelerated if appropriate online basis functions are constructed and appropriate number of offline basis functions are used. The construction of online basis functions relies on analysis and the choice of the offline basis functions. In this paper, we (1) develop analysis for GMsFEM for perforated domains (2) design procedures for constructing online multiscale basis functions (3) present analysis of online multiscale procedures (4) develop adaptive procedures (5) present numerical results. By using a computable error indicator, we locate regions, where enrichment is necessary, and construct new online basis functions in order to improve the accuracy. Our numerical results for the elasticity equation and the Stokes system show that the method has an excellent performance and rapid convergence. In particular, only a few online basis functions in some selected regions improve the accuracy of the solution. Our analysis shows that the convergence rate depends on the number of offline basis functions, and one can obtain a fast convergence by including enough offline basis functions. This convergence theory can also be applied to the Laplace equation and the elasticity equation. One possible future direction is the goal-oriented adaptivity [19], in which basis functions are added in order to reduce the goal error.

7 Acknowledgement

YE's work is partially supported by the U.S. Department of Energy Office of Science, Office of Advanced Scientific Computing Research, Applied Mathematics program under Award Number DE-FG02-13ER26165 and the DoD Army ARO Project and NSF (DMS 0934837 and DMS 0811180). Eric Chung's research is partially supported by Hong Kong RGC General Research Fund (Project: 400813) and CUHK Faculty of Science Research Incentive Fund 2015-16. MV's work is partially supported by Russian Science Foundation Grant RS 15-11-10024 and RFBR 15-31-20856.

References

- [1] G. ALLAIRE, *Homogenization of the navier-stokes equations in open sets perforated with tiny holes ii: Non-critical sizes of the holes for a volume distribution and a surface distribution of holes*, Archive for Rational Mechanics and Analysis, 113 (1991), pp. 261–298.
- [2] G. ALLAIRE AND R. BRIZZI, *A multiscale finite element method for numerical homogenization*, SIAM J. Multiscale Modeling and Simulation, 4 (2005), pp. 790–812.
- [3] G. ALLAIRE AND H. HUTRIDURGA, *Upscaling nonlinear adsorption in periodic porous media—homogenization approach*, Applicable Analysis, (2015), pp. 1–36.
- [4] I. BABUŠKA, V. NISTOR, AND N. TARFULEA, *Generalized finite element method for second-order elliptic operators with Dirichlet boundary conditions*, J. Comput. Appl. Math., 218 (2008), pp. 175–183.
- [5] Z. BARE, J. ORLIK, AND G. PANASENKO, *Non homogeneous dirichlet conditions for an elastic beam: an asymptotic analysis*, Applicable Analysis, (2015), pp. 1–12.
- [6] A. Y. BELIAEV AND S. KOZLOV, *Darcy equation for random porous media*, Communications on pure and applied mathematics, 49 (1996), pp. 1–34.
- [7] D. L. BROWN AND D. PETERSEIM, *A multiscale method for porous microstructures*, arXiv preprint arXiv:1411.1944, (2014).

- [8] V. CALO, Y. EFENDIEV, J. GALVIS, AND G. LI, *Randomized oversampling for generalized multiscale finite element methods*, arXiv preprint, arXiv: 1409.7114, (2014).
- [9] L. CAO, *Multiscale asymptotic expansion and finite element methods for the mixed boundary value problems of second order elliptic equation in perforated domains*, Numerische Mathematik, 103 (2006), pp. 11–45.
- [10] L. CAO, Y. ZHANG, W. ALLEGRETTO, AND Y. LIN, *Multiscale asymptotic method for Maxwell’s equations in composite material*, SIAM J. Numer. Anal., 47(6) (2010), pp. 4257–4289.
- [11] H. Y. CHAN, E. T. CHUNG, AND Y. EFENDIEV, *Adaptive mixed GMsFEM for flows in heterogeneous media*, arXiv preprint arXiv:1507.01659, (2015).
- [12] C.-C. CHU, I. G. GRAHAM, AND T.-Y. HOU, *A new multiscale finite element method for high-contrast elliptic interface problems*, Math. Comp., 79 (2010), pp. 1915–1955.
- [13] E. CHUNG, Y. EFENDIEV, AND C. LEE, *Mixed generalized multiscale finite element methods and applications*, SIAM Multiscale Model. Simul., 13 (2014), pp. 338–366.
- [14] E. CHUNG, W. T. LEUNG, AND M. VASILYEVA, *Mixed GMsFEM for second order elliptic problem in perforated domains*, unpublished, (2014).
- [15] E. T. CHUNG, Y. EFENDIEV, AND W. T. LEUNG, *An online generalized multiscale discontinuous galerkin method (GmsDGM) for flows in heterogeneous media*, arXiv preprint arXiv:1504.04417, (2015).
- [16] E. T. CHUNG, Y. EFENDIEV, AND W. T. LEUNG, *Residual-driven online generalized multiscale finite element methods*, Journal of Computational Physics, 302 (2015), pp. 176–190.
- [17] E. T. CHUNG, Y. EFENDIEV, AND G. LI, *An adaptive GmsFEM for high contrast flow problems*, J. Comput. Phys., 273 (2014), pp. 54–76.
- [18] E. T. CHUNG, Y. EFENDIEV, G. LI, AND M. VASILYEVA, *Generalized multiscale finite element method for problems in perforated heterogeneous domains*, Applicable Analysis, 255 (2015), pp. 1–15.
- [19] E. T. CHUNG, W. T. LEUNG, AND S. POLLOCK, *Goal-oriented adaptivity for GmsFEM*, Journal of Computational and Applied Mathematics, (2015), pp. 625–637.
- [20] W. E AND B. ENGQUIST, *Heterogeneous multiscale methods*, Comm. Math. Sci., 1 (2003), pp. 87–132.
- [21] Y. EFENDIEV, J. GALVIS, AND T. HOU, *Generalized multiscale finite element methods (gmsfem)*, Journal of Computational Physics, 251 (2013), pp. 116–135.
- [22] Y. EFENDIEV, J. GALVIS, G. LI, AND M. PRESCHO, *Generalized multiscale finite element methods. oversampling strategies*, International Journal for Multiscale Computational Engineering, 12(6) (2014), pp. 465–484.
- [23] Y. EFENDIEV AND T. HOU, *Multiscale Finite Element Methods: Theory and Applications*, vol. 4 of Surveys and Tutorials in the Applied Mathematical Sciences, Springer, New York, 2009.
- [24] T. FRATROVIĆ AND E. MARUŠIĆ-PALOKA, *Nonlinear brinkman-type law as a critical case in the polymer fluid filtration*, Applicable Analysis, (2015), pp. 1–22.
- [25] R. P. GILBERT AND M.-J. OU, *Acoustic wave propagation in a composite of two different poroelastic materials with a very rough periodic interface: a homogenization approach*, International Journal for Multiscale Computational Engineering, 1 (2003).
- [26] R. P. GILBERT, A. PANCHENKO, AND A. VASILIC, *Acoustic propagation in a random saturated medium: the biphasic case*, Applicable Analysis, 93 (2014), pp. 676–697.

- [27] R. P. GILBERT, A. PANCHENKO, AND X. XIE, *A prototype homogenization model for acoustics of granular materials*, International Journal for Multiscale Computational Engineering, 4 (2006).
- [28] M. GRIEBEL AND M. KLITZ, *Homogenization and numerical simulation of flow in geometries with textile microstructures*, Multiscale Modeling & Simulation, 8 (2010), pp. 1439–1460.
- [29] P. HENNING AND M. OHLBERGER, *The heterogeneous multiscale finite element method for elliptic homogenization problems in perforated domains*, Numerische Mathematik, 113 (2009), pp. 601–629.
- [30] T. HOU AND X. WU, *A multiscale finite element method for elliptic problems in composite materials and porous media*, J. Comput. Phys., 134 (1997), pp. 169–189.
- [31] O. ILIEV, R. KIRSCH, Z. LAKDAWALA, S. RIEF, AND K. STEINER, *Modeling and simulation of filtration processes*, in Currents in Industrial Mathematics, Springer, 2015, pp. 163–228.
- [32] O. ILIEV, Z. LAKDAWALA, AND V. STARIKOVICIUS, *On a numerical subgrid upscaling algorithm for stokes-brinkman equations*, Computers & Mathematics with Applications, 65 (2013), pp. 435–448.
- [33] O. ILIEV, R. LAZAROV, AND J. WILLEMS, *Variational multiscale finite element method for flows in highly porous media*, Multiscale Model. Simul., 9 (2011), pp. 1350–1372.
- [34] V. V. JIKOV, S. M. KOZLOV, AND O. A. OLEINIK, *Homogenization of Differential Operators and Integral Functionals*, Springer-Verlag, 1991.
- [35] L. LE BRIS, F. LEGOLL, AND A. LOZINSKI, *An MsFEM type approach for perforated domains*, Multiscale Modeling & Simulation, 12(3) (2014), pp. 1046–1077.
- [36] V. MAZ’YA AND A. MOVCHAN, *Asymptotic treatment of perforated domains without homogenization*, Mathematische Nachrichten, 283 (2010), pp. 104–125.
- [37] V. MAZ’YA, A. MOVCHAN, AND M. NIEVES, *Green Kernels and Meso-Scale Approximations in Perforated Domains*, Springer-Berlin, Lecture Notes in Mathematics, 2077, 2013.
- [38] A. MUNTEAN, M. PTASHNYK, AND R. E. SHOWALTER, *Analysis and approximation of microstructure models*, Applicable Analysis, 91 (2012), pp. 1053–1054.
- [39] M. OHLBERGER AND F. SCHINDLER, *Error control for the localized reduced basis multi-scale method with adaptive on-line enrichment*, arXiv preprint arXiv:1501.05202, (2015).
- [40] O. A. OLEINIK AND T. A. SHAPOSHNIKOVA, *On the homogenization of the poisson equation in partially perforated domains with arbitrary density of cavities and mixed type conditions on their boundary*, Atti della Accademia Nazionale dei Lincei. Classe di Scienze Fisiche, Matematiche e Naturali. Rendiconti Lincei. Matematica e Applicazioni, 7 (1996), pp. 129–146.
- [41] I. PANKRATOVA AND K. PETTERSSON, *Spectral asymptotics for an elliptic operator in a locally periodic perforated domain*, Applicable Analysis, 94 (2015), pp. 1207–1234.
- [42] E. SÁNCHEZ-PALENCIA, *Non-homogeneous media and vibration theory*, in Non-homogeneous media and vibration theory, vol. 127, 1980.
- [43] B. VERLEYE, R. CROCE, M. GRIEBEL, M. KLITZ, S. V. LOMOV, G. MORREN, H. SOL, I. VERPOEST, AND D. ROOSE, *Permeability of textile reinforcements: Simulation, influence of shear and validation*, Composites Science and Technology, 68 (2008), pp. 2804–2810.